Published in final edited form as:
Dev Dyn. 2011 September ; 240(9): 2175–2193. doi:10.1002/dvdy.22711.

Hedgehog signaling in the posterior region of the mouse gastrula suggests manifold roles in the fetal-umbilical connection and posterior morphogenesis

Jacob M. Daane and **Karen M. Downs***
Department of Cell and Regenerative Biology, University of Wisconsin-Madison School of Medicine and Public Health, 1300 University Avenue, Madison, WI 53706

SUMMARY

Although many fetal birth defects, particularly those of the body wall and gut, are associated with abnormalities of the umbilical cord, the developmental relationship between these structures is largely obscure. Recently, genetic analysis of mid-gestation mouse embryos revealed that defects in Hedgehog signaling led to omphalocoele, or failure of the body wall to close at the umbilical ring (Matsumaru et al., 2011). However, systematic spatiotemporal localization of Hedgehog signaling in the allantois, or umbilical precursor tissue, and the surrounding regions has not been documented. Here, a combination of reagents, including the *Ptc1:lacZ* and *Runx1:lacZ* reporter mice, immunohistochemistry for Smoothened (Smo), Sonic Hedgehog (Shh), and Indian hedgehog (Ihh), and detailed PECAM-1/Flk-1/Runx-1 analysis, revealed robust Hedgehog signaling in previously undocumented posterior sites over an extended period of time (~7.0–9.75 dpc). These included the recently described proximal walls of the allantois (Ventral and Dorsal Cuboidal Mesothelia; VCM and DCM, respectively); the ventral embryonic surface continuous with them; hemogenic arterial endothelia; hematopoietic cells; the hindgut; ventral ectodermal ridge (VER); chorionic ectoderm; and the intraplacental yolk sac (IPY), which appeared to be a site of placental hematopoiesis. This map of Hedgehog signaling in the posterior region of the mouse conceptus will provide a valuable foundation upon which to elucidate the origin of many posterior midline abnormalities, especially those of the umbilical cord and associated fetal defects.

Keywords

allantois; amnion; body wall; dorsal aortae; Dorsal Cuboidal Mesothelium (DCM); Flk-1; Hedgehog; hindgut; intraplacental yolk sac (IPY); mouse; Oct-3/4; omphalocoele; omphalomesenteric artery; PECAM-1; placenta; primitive streak; Sinuses of Duval; somatopleure; splanchnopleure; umbilical cord; Ventral Cuboidal Mesothelium (VCM); Ventral Ectodermal Ridge (VER); vessel of confluence (VOC); visceral endoderm; yolk sac

INTRODUCTION

At least half of all umbilical defects are associated with abnormalities in posterior fetal organs, suggesting the existence of an intimate developmental relationship between the fetus and its vital umbilical conduit to the mother (Stevenson and Hall, 2006). However, as the umbilical cord has been discarded in most experimental investigations and embryological collections (Carter, 2007), important morphological and molecular information that could reveal the developmental relationship between the fetus and its umbilical cord has

*Corresponding author: kdowns@wisc.edu.

unfortunately been forfeited. Consequently, many umbilical-associated fetal posterior defects have been assigned to the non-specific category of “orphan diseases” (http://rarediseases.info.nih.gov/); these include omphalocoele, gastroschisis, body wall defects, sirenomelia, imperforate anus, and Cantrell pentalogy.

In this study, we have investigated the whereabouts of Hedgehog signaling in the umbilical precursor, called the allantois, and surrounding tissues, including the posterior region of the fetus. Hedgehog was selected because of its association with defects of the embryonic midline (Chiang et al., 1996; Roessler et al., 1996), particularly those involving the notochord, or anterior extension of the primitive streak. Recent results have suggested that the allantois, common to all amniotes, is a posterior midline appendage formed by extension of the primitive streak into the extraembryonic region (Downs et al., 2009). There, the extraembryonic streak creates a cell reservoir, the allantoic core domain (ACD), critical for allantoic bud formation, elongation to the chorion, and vascularization (Downs et al., 1998; Inman and Downs, 2006; Downs et al., 2009).

Previous studies had shown that abrogation of Hedgehog signaling affects vascularization of the yolk sac but not that of the allantois (Astorga and Carlsson, 2007); from this, the authors concluded that allantoic vascularization is distinctly different from other vascular systems. However, while allantoic vascularization was not dependent upon Hedgehog, the authors did not provide information on the location of Hedgehog in the allantois, and did not consider a potential role for Hedgehog signaling in other aspects of allantoic vascularization, for example, patterning and hematopoiesis.

The nascent allantoic artery is stereotypically patterned (Naiche and Papaioannou, 2003; Inman and Downs, 2006). Distally, it consists of a highly branched network of Flk-1 (Downs et al., 1998) and PECAM-1 (Inman and Downs, 2006)-positive endothelial cells that spread over the chorion and become part of the labyrinth, or site of fetal-maternal exchange. Proximally, the relatively unbranched nascent artery is directly aligned with the primitive streak, or midline of the future embryonic body; it amalgamates with the prospective visceral yolk sac omphalomeseneteric artery (OA) and fetal dorsal aortae at a single site, which we have provisionally called the “vessel of confluence” (VOC) (Inman and Downs, 2007). Fetal blood is collected from far-flung embryonic sites and efficiently channeled to and from the labyrinth via the VOC. Although the processes of chorio-allantoic union and vascularization of the chorionic plate are controlled at multiple genetic levels (reviewed in (Rossant and Cross, 2001; Cross et al., 2003; Cross, 2005; Inman and Downs, 2007), the mechanism by which the umbilical vasculature becomes patterned and patent with the other major circulatory systems of the conceptus is not known. In addition, the allantois exhibits definitive hematopoietic potential (Zeigler et al., 2006; Corbel et al., 2007), but the location of allantoic hematopoietic niches, if they exist, is obscure.

Recently, we discovered that the outer surface of the murine allantois, called the “mesothelium”, is regionally functionally distinct (Daane et al., 2011), which led to a model in which allantoic mesothelium mediates vascular patterning within the nascent umbilical cord. Specifically, passage of small molecules into the allantois from the exocoelom and/or associated tissues, e.g., the yolk sac, amnion and chorion, may promote distal vascular branching through the porous distal mesothelium. By contrast, the relatively impermeable Ventral Cuboidal Mesothelium (VCM), which overlies the nascent umbilical artery and vessel of confluence, may prevent proximal branching, ensuring that fetal blood is channeled through the VOC. Although the signaling pathways in this model have not yet been identified, defective Hedgehog signaling was recently shown to be involved in omphalocoele, a defect of the umbilical ring and associated body wall of the fetus (Matsumaru et al., 2011).

To discover whether the proximal allantoic walls were developmentally, physically, and/or molecularly associated with the fetal body walls, we set out to create a systematic blueprint of sites of Hedgehog signaling during the emergence of the allantois and posterior region of the mouse conceptus, which included the proximal allantoic walls, the embryonic body walls, visceral yolk sac and OA, the amnion and the hindgut. All of these are associated with various umbilical defects, including omphalocoele (Stevenson and Hall, 2006). Al;though previous studies focused on Ptc-1, Shh and Ihh expression in the embryo proper at widely-spaced intervals (8.0–16.5 dpc; (Bitgood and McMahon, 1995; Goodrich et al., 1995), the yolk sac and chorio-allantoic labyrinth (8.5–13.5 dpc; (Jiang and Herman, 2006), and/or the anterior region of the developing fetus (Epstein et al., 1999), to the best of our knowledge, localization of Hedgehog signaling proteins at closely spaced intervals has not been carried out during posterior morphogenesis and establishment of the fetal-umbilical connection. Our results implicate possible new roles for Hedgehog signaling in development of the umbilical and fetal body walls, hindgut, posterior arterial system, and hematopoiesis.

RESULTS AND DISCUSSION

Developmental phases and general experimental strategy

Development of the posterior region of the murine conceptus was parsed into three anatomical phases based on the relationship between the allantois, extraembryonic tissues, and the embryo/fetus (Table 1). The focus in this study was on localization of Ptc-1, the major receptor of all Hedgehog ligands. Binding of secreted Hedgehog to Ptc-1 relieves inhibition of Smoothened, a G-protein-coupled receptor that activates downstream intracellular components of the pathway, leading to morphogenetic organization during embryogenesis (reviewed in (Wilson and Chuang, 2010). To verify association of Ptc-1 with these signaling partners, we included experiments that examined the relationship between Smoothened (Smo), and the signaling ligands, Sonic hedgehog (Shh) and Indian hedgehog (Ihh) with Ptc-1. In addition, correlation of Ptc-1 with posterior vascularization and hematopoiesis was made by PECAM-1 immunostaining (Newman, 1997), use of the *Flk1:lacZ* reporter mouse (Shalaby et al., 1995) and the *Runx1:lacZ* reporter mouse (North et al., 2002).

Modification of X-gal staining solutions increased the sensitivity of the Ptc-1:lacZ and Runx1:lacZ reporters

To localize Ptc-1, we modified a standard X-gal staining protocol (Table 2, and Materials and Methods). In the standard reaction, galactose is cleaved from X-gal by β-galactosidase, expressed here from the *Ptc1* promoter, producing a colorless product (5-bromo-4-chloro-indoxyl) that non-enzymatically dimerizes into a blue precipitate (Holt and Sadler, 1958). Dimerization is an oxidation reaction that requires electron acceptors of a certain redox potential, and is fulfilled by $K_3Fe(CN)_6$ and $K_4Fe(CN)_6.3H_2O$ (Lojda, 1970) (5 mM each, Table 2). In addition, $K_3Fe(CN)_6$ stimulates precipitation of the X-gal cleavage product while $K_4Fe(CN)_6$ prevents oxidation of the colored precipitate into a colorless compound (Dannenberg and Suga, 1981; Poulsen et al., 1997).

The standard protocol produced an X-gal precipitate whose intensity ranged from dark blue throughout the cells of the allantoic VCM, associated yolk sac endoderm/mesoderm, yolk sac mesothelium, and some cells of the node, to barely perceptible punctate blue in the core cells of the allantois, yolk sac mesothelia and chorionic mesoderm (Fig. 1A, D, G, H, and data not shown). In addition to dark blue staining at the end of the reaction period, we noted a purple-pink color over the yolk sac and allantois, which suggested that some blue precipitate was oxidizing with concomitant loss of signal (data not shown).

Thus, to provide more certainty of *Ptc1* expression in sites of punctate staining, we explored several scenarios in which the molarity of each iron component was doubled and used independently of the other (Table 2; Fig. 1B, C, E, F, I- L). We found that 10 mM $K_4Fe(CN)_6$-$3H_2O$ together with unchanged concentrations of $MgCl_2$ and X-gal both enhanced the X-gal precipitate, especially in the VCM and allantoic core (Fig. 1C, K, L), and both components of the node (Fig. 1F); by contrast, 10 mM $K_3Fe(CN)_6$ decreased it (Fig. 1B, E, I, J). We therefore concluded that some signal was lost in the standard X-gal protocol through oxidation. Unless otherwise indicated (see Materials and Methods), 10 mM $K_4Fe(CN)_6$-$3H_2O$, which produced the most intense blue precipitate, was used throughout this study, and also with the *Runx1:lacZ* reporter mouse line. Short staining times (6 hours) for both Ptc-1 and Runx-1 appeared to identify the most robust localization sites, while longer periods brought out additional sites of lower level expression. Further, while we noticed no increasing intensity in X-gal staining beyond 13 hours in the *Ptc:lacZ* reporter, intensity of X-gal staining increased between 12–20 hours in the *Runx1:lacZ* reporter, described in the appropriate section. Finally, we noted that a few giant cells of reporter-negative conceptuses took up X-gal precipitate only in the scenario where 10 mM $K_4Fe(CN)_6$-$3H_2O$ was used (1/15 conceptuses at 8.0 dpc; 2/9 at 9.0 dpc; 4/4 at 9.75 dpc; data not shown).

Hedgehog signaling and its relation to the nascent allantoic vasculature

Developmental Phase I (Neural plate/No allantoic bud (OB) -Headfold stages, ~7.0–8.0 dpc)—At the neural plate/no allantoic bud (OB)-Neural plate/Early Bud (EB) stages (~7.0–7.25 dpc), Ptc-1 was heaviest in a circumferential ring at the embryonic/extraembryonic boundary (Fig. 2A). Histological examination revealed weak Ptc-1 in visceral endoderm, both layers of the chorion and amnion, and the proamniotic tube, while heaviest Ptc-1 localized to the entire nascent allantoic bud, and extended into the adjacent mesoderm of the visceral yolk sac (Fig. 2B). Ptc-1 was not present in the anterior embryonic node (Fig. 2A), but emerged there by the EB stage (Fig. 2C, D); at this and all subsequent stages through 6-s, when examination of the node ended, Ptc-1 was found in both the ventral and dorsal components of the node (Fig. 2C, D, N). In the allantoic bud, Ptc-1 localized most robustly to the nascent VCM and was emerging within the associated endodermal and mesodermal components of the visceral yolk sac (Fig. 2E).

By the Early Headfold (EHF) stage (~7.75 dpc), Ptc-1 increased in intensity in the allantois and node. While present now in the notochord, Ptc-1 was not observed in the embryonic primitive streak (located between the node and the base of the allantois; Fig. 2F, and data not shown). Ptc-1 was weakly present throughout the core of the allantois, and within the amnion-associated DCM (Fig. 2G). Allantoic Ptc-1 was particularly robust in the VCM and adjacent yolk sac mesoderm/endoderm, creating a “V”-shape at this intersection (Fig. 2G), which was distal to the more weakly-stained allantois-associated extraembryonic visceral endoderm (“AX”), and which plays a role in establishing the allantoic bud (Downs et al., 2009). Thus, allantois-associated visceral endoderm is compartmentalized into distinct regions.

We next asked whether the Ptc-1 receptor was associated with the Hedgehog signaling components, Smo, Shh, and Ihh. For this, immunohistochemistry was initiated at headfold stages (Fig. 2H–S). Smo, Shh, and, to a lesser extent, Ihh, localized to visceral endoderm, both embryonic and extraembryonic, as well as to several underlying cell layers (Fig. 2H, J, L), including the primitive streak, embryonic mesoderm, visceral yolk sac mesoderm, associated blood islands, and the cardiac field. All three proteins were found in the ventral layer of the node and notochord (e.g., Fig. 2O). Why Ptc-1 localization was found the dorsal component of the node (Fig. 2N) while Smo was not is not clear, as both Shh and Ihh were

also observed in the dorsal component (data not shown). This discrepancy may be explained by results of recent studies which have put forth evidence for non-canonical Hedgehog signaling independent of Smoothened (Jenkins, 2009; Chang et al., 2010).

Smo, Shh, and Ihh proteins were found in allantoic cells internal to the AX beneath the VCM. However, in contrast to the *Ptc1:lacZ* reporter, Smo, Shh and Ihh were observed in the embryonic component of the primitive streak (compare Fig. 2F, G with Fig. 2H–M). As reactions lacking these antibodies revealed no background staining (data not shown), it was not clear why their cognate proteins were found in the embryonic streak while Ptc-1 was not. Shh is thought to form a major signaling complex with Ptc-2 (Motoyama et al., 1998), which was discovered after Ptc-1 (Takabatake et al., 1997; Motoyama et al., 1998). Thus, one possibility is that Ptc-2 is the predominant Hedgehog receptor in the embryonic streak. Expression of Ptc-2 has not yet been reported at the stages under scrutiny here. At this and all subsequent stages, the amnion variously contained Hedgehog signaling elements (data not shown).

Finally, at the EB stage, Ptc-1 was weakly present in the lateral edges of chorionic ectoderm, which is complexed with extraembryonic visceral and parietal endoderm at sites of formation of the future Sinuses of Duval, composed of extraembryonic endoderm that creates the intraplacental yolk sac (IPY) (Duval, 1892) (Fig. 2P). At the EHF stage, Ptc-1, Smo and Shh were also found in this site (Fig. 2Q–S), while Ihh was much less intense here, if present at all (data not shown).

Developmental Phase II (1–9-somite pair (-s) stages, ~8.0–8.75 dpc)— Overlapping sites of Hedgehog localization continued throughout Phase II (1–9-s stages, ~8.0–8.75 dpc). Ptc-1 (Fig. 3A–F), Smo (Fig. 3G–I), Shh (Fig. 3J–L) and Ihh (Fig. 3M-O) were consistently most robust in the intimately associated allantoic VCM and adjoining visceral yolk sac mesoderm/endoderm (e.g., Fig. 3E, I, M). By 3–4-s, Ptc-1, Smo and Shh had noticeably spread to the allantoic core domain, or ACD (Fig. 3C, F, I–K). Ptc-1 was weak in the hindgut invagination (Fig. 3C, E, F); by contrast, Smo, Shh and Ihh were all robustly expressed there (Fig. 3I, L–O). Ptc-1, Smo, Shh, and now Ihh were all evident within the lateral edges of chorionic ectoderm (data not shown).

To relate Hedgehog signaling to the emerging posterior vasculature, we clarified the relationship between Flk-1 and PECAM-1 within the allantois. Previous results had suggested that Flk-1 and PECAM-1, both found in nascent endothelial cells (Yamaguchi et al., 1993; Newman and Newman, 2003), might identify common as well as distinct allantoic precursor cells (Downs et al., 1998; Inman and Downs, 2006). At the bud stages, PECAM-1 and Flk-1, like Ptc-1, were scattered throughout the allantois (Fig. 4A–C); PECAM-1 was also found in cells immediately internal to the AX (Fig. 4A, C).

By headfold stages, PECAM-1 localized to a midline file of cells (Fig. 4D) which also co-localized Flk-1 (e.g., Fig. 4E); this file extended through the allantois from the site of insertion of the Ventral Cuboidal Mesothelium (VCM) into the yolk sac (e.g., Fig. 4F) to the distal tip of the allantois (Fig. 4D). PECAM-1/Flk-1 double- positive cells also localized diffusely to the DCM and amnion (Fig. 4G) where Ptc-1 was relatively low (data not shown).

Over time, the proximal PECAM-1/Flk-1-positive allantoic artery thickened beneath the Ptc-1-rich VCM (Fig. 4H, I); in addition, the vessel of confluence became evident beneath the allantoic VCM (Fig. 4J, K). The vessel of confluence was positive for both Flk-1 and PECAM-1 (Fig. 4J), and was associated with relatively high levels of Ptc-1 (Fig. 4K). As a general rule, Flk-1-positive cells were often not co-stained with PECAM-1 (e.g., Fig. 4J),

while PECAM-1-positive cells always exhibited Flk-1. Amalgamation between the arterial systems of the allantois, yolk sac, and fetal embryonic dorsal aortae took place at the vessel of confluence (VOC) by 5–6-s (Fig. 4I, L). Then, while the allantoic portion of the VOC remained associated with the allantois, the embryonic portion was transformed into the omphalomeseneteric artery (OA), elongating in tandem with the hindgut (Fig. 4L, M). Two anastomosing endothelial branches were observed at right angles to the OA and paired dorsal aortae (Fig. 4M); at a slightly later stage, these communications are sites of hematopoiesis (Zovein et al., 2010).

PECAM-1 and Flk-1 within the VOC and nascent umbilical artery was associated with the robustly Hedgehog-positive VCM (Fig. 2), suggesting a potentially important relationship between Hedgehog signaling and posterior arterialization, further explored, below.

Developmental Phase III (10–27-s, ~8.75–9.75 dpc)—Phase III encompassed two subperiods (Table 1): Phase IIIa: 10–18-s (~8.75–9.25 dpc) (Fig. 5), and Phase IIIb: 23–27-s (~9.75 dpc) (Fig. 6).

During Phase IIIa, the tailbud enlarged. The hindgut tube and OA tandemly formed with posterior-anterior polarity. The dorsal (DCM) and ventral (VCM) allantoic walls became posterior (DCM) and anterior (VCM) umbilical walls, respectively, and contiguous with the embryonic ventral body surface (Fig. 5A, B), whose nature, in the mouse, is obscure. In humans, the primary ventral caudal body wall consists of two symmetrical lateral and two mid-ventral folds that converge and close at the umbilical ring (Brewer and Williams, 2004). The lateral folds are continuous with the amnion while the mid-caudal folds overlie the hindgut and omphalomeseneteric artery.

The developmental sequence of hindgut and omphalomeseneteric artery formation (Fig. 5C–H) revealed that extraembryonic endoderm of the visceral yolk sac, associated blood vessels, and splanchnopleure closed over exposed gut endoderm (Fig. 5C–E), creating the omphalomeseneteric artery, hindgut tube, and the epithelial surface of both of these structures (Fig. 5F–H). Ptc-1 was present in all of these sites, including many associated hematopoietic cells. Ptc-1 persisted in the VCM/anterior umbilical wall (Fig. 5I, J) and now appeared at relatively high levels in the DCM/posterior umbilical wall and lateral somatopleure. Together, umbilical walls, splanchnopleure and somataopleure formed the umbilical ring, which was continuous with the embryonic ventral surface of the embryo (Fig. 5I–K). Both umbilical walls squarely overlay the vessel of confluence, a fixed point at which the umbilical, omphalomeseneteric, and dorsal aortae communicated. The posterior vascular relationship is beautifully illustrated in 3-D reconstruction panels in a recent study, though the vessel of confluence per se was not indicated (Walls et al., 2008).

By Phase IIIb (~23–27-s; 9.75 dpc) (Fig. 6A, B), that part of the omphalomeseneteric artery (OA) extending from the hindgut to the extraembryonic visceral endoderm of the yolk sac contained solid masses of Ptc-1-positive cells (Fig. 6B), which are hematopoietic stem cell niches (Garcia-Porrero et al., 1995). Ptc-1 was no longer detectable in the somatopleure component of the lateral body wall at the umbilical ring (Fig. 6B–D), but persisted throughout the hindgut, within the splanchnopleuric surface overlying it and the OA (Fig. 6B–F), the endothelium of the OA along its full length (Fig. 6B, and data not shown), the anterior (Fig. 6C, D) and posterior umbilical walls (Fig. 6E), and the ventral ectodermal ridge (VER) (Fig. 6F), a remnant of the primitive streak.

Thus, Hedgehog is found in the mid-ventral surface of the mouse embryo, especially that region associated with the allantois. This conclusion is consistent with defects in Hedgehog signaling at the umbilical ring of the mid-gestation fetus (Matsumaru et al., 2011). In

addition, mutants in Gli2, a downstream Hedgehog effector, exhibit diaphragmatic hernia, and Gli3 mutants exhibit omphalocoele (Brewer and Williams, 2004). A cursory examination of Ptc-1 in whole 13.0 dpc fetuses revealed a persistent, and strong relationship between the herniated midgut and the site of umbilical insertion there (Fig. 7A, B), and persistent Ptc-1 in the placenta, in accord with previous findings (Jiang and Herman, 2006) (Fig. 7C).

Finally, Ptc-1 was also found in the endothelium and many associated hematopoietic cells of the OA and dorsal aorta (e.g., Fig. 6G), the visceral yolk sac (Fig. 6H), and within the presumptive intraplacental yolk sac (IPY) (Fig. 6I). Together, these data reveal strong association between arterial endothelium of the posterior region, hematopoiesis, and Hedgehog signaling. Previous results have identified Hedgehog signaling in the ventral compartment of the dorsal aortae (Peeters et al., 2009), as well as within the IPY at 11–13 dpc (Jiang and Herman, 2006). Association of Ptc-1 with sites of hematopoiesis during these early stages, especially in the nascent umbilical artery and presumptive IPY, will be explored in the next section.

Spatiotemporal resolution of Runx1 within the allantois and surrounding regions

Prior to their union to form the chorio-allantoic placenta, the allantois and chorion have definitive hematopoietic potential (Zeigler et al., 2006; Corbel et al., 2007); however, whether these two tissues give rise to definitive hematopoietic cells in vivo is not known. In light of our findings, which showed the presence of Ptc-1 in blood cells and hemogenic arteries, we systematically re-visited Runx-1 localization in the allantois and surrounding regions, using the *Runx1:lacZ* reporter mouse. For this, we focused on Phases II and III, when the arterial vasculatures were forming, merging and exhibiting signs of hematopoiesis. Although Runx-1 may not be specific to hematopoietic cells, having been previously described in the visceral endoderm of the mouse yolk sac (North et al., 1999; Zeigler et al., 2006), nevertheless, a wide-range of definitive hematopoietic precursor cells are thought to express *Runx1* (reviewed in (Swiers et al., 2010).

X-gal-staining in the *Runx1:lacZ* reporter mouse over shorter time periods allowed visualization of the strongest Runx-1 regions. For example, after 6–12 hours, we discovered that, prior to 4-s pairs, the distal allantois contained the most Runx-1 (Fig. 8A–D). By contrast, the nascent vessel of confluence was most robustly Runx-1 positive at 4-s (Fig. 8E–G). At all stages, the visceral yolk sac was positive, and included the visceral endoderm, blood vessels, most hematopoietic cells, and mesothelium (Fig. 8A–H). The lateral edges of the chorionic ectoderm were more strongly positive than the central region, while all of the chorionic mesoderm was robustly Runx-1-positive (Fig. 8H). Runx1-positive cells of the vessel of confluence appeared to contain PECAM-1 (Fig. 8I–K); Runx-1-positive cells were also associated with the unbranched PECAM-1-positive component of the allantoic artery (Fig. 8).

Examination of some specimens within Phase IIIa (~10–14-somite pairs) revealed that Runx-1 often overlapped sites of Ptc-1, appearing consistently to be budding from the endothelium of the OA where the latter connects the hindgut to the yolk sac (Fig. 9A, B). During hindgut closure and OA formation (Fig. 9C–F), Runx-1 was found in the yolk sac endoderm and in hematopoietic cells of yolk sac blood vessels (Fig. 9C–F), similar to Ptc-1 (Fig. 5). Unlike Ptc-1, however, the point of hindgut closure and OA formation did not contain detectable Runx-1 (Fig. 9C, D). Like Ptc-1, Runx-1-positive cells were found in the following similar sites and at similar levels to Ptc-1: the vessel of confluence and umbilical artery (Fig. 9G, H), VCM/anterior wall of the umbilical cord (Fig. 9G, H), near the umbilical veins (Fig. 9I), DCM/posterior umbilical wall (Fig. 9J), within the nascent ventral ectodermal ridge (VER) (Fig. 9K), and the nascent Sinuses of Duval (Fig. 9L).

Phase IIIb specimens (23–27-s; ~9.75 dpc) provided more striking examples of the aforementioned sites of Runx-1. Large clusters of Runx-1 hematopoietic cells appeared to be budding from arterial endothelium of the OA (Fig. 10A, B), they persisted at the interface between general yolk sac visceral endoderm and blood vessels (Fig. 10C, D), they were occasionally found within loose mesenchyme of the lateral body wall (Fig. 10E) and chorionic labyrinth (Fig. 10F), and clearly within the IPY both as part of the sinus wall and as blood cells (Fig. 10H, I). Finally, Runx-1 appeared to be present in the hair follicles of the mouse ear, tissue of which was used to genotype weanlings for Runx-1 status (data not shown). Intriguingly, the latter observation is consistent with hair follicle CD34, a stem and progenitor cell marker found in many hematopoietic cells (Trempus et al., 2003).

Removal of the allantois results in re-establishment of the VCM, DCM, and nascent allantoic hemogenic arterial vessel within allantoic regenerates

Previous results from our laboratory had shown that, although allantoises failed to elongate after microsurgical removal of the allantoic core domain (ACD), they nevertheless exhibited a correctly patterned nascent vasculature, vessel of confluence (VOC), and amalgamation at the VOC (Downs et al., 2009). This suggested that the source of vascular patterning signals lay outside the ACD (Downs et al., 2009). As the aforementioned data demonstrated association of Ptc-1 with the nascent umbilical artery and vessel of confluence, we asked whether the VCM and/or DCM could be implicated in restoration of a correctly patterned umbilical artery. For this, the allantois was removed between headfold and 2-s stages; allantoic regenerates were then examined for reformation of the VCM/DCM and the status of the nascent umbilical artery.

First, the site from which the allantois had been aspirated was examined prior to culture (Fig. 11A–C). PECAM-1 was observed between the outer visceral endoderm and the posterior embryonic tissue (Fig. 11A), as described in Fig. 4. Afadin, which localized strongly to the VCM (Daane et al., 2011) (Fig. 11C) and Ptc-1 (Fig. 11C) were not discernible at any stage in the remaining region. After culture, both the DCM, as indicated by alpha-4-integrin (Fig. 11D), and VCM (Fig. 11E) had re-formed, as indicated by high levels of afadin (Fig. 11E) and Ptc-1 (Fig. 11F). In all regenerates, the unbranched and correctly patterned PECAM-1 vessel was present (Fig. 11G), and in most of these, Runx-1-positive cells were localized to this vessel (Fig. 11G).

Given that the VCM was restored along with the allantoic artery and Runx-1 cells, these results are consistent with a role of the VCM, and possibly Ptc-1, in patterning the umbilical vasculature. Previous results suggested that Hedgehog signaling was indispensable for yolk sac vasculogenesis, but dispensable for that in the allantois, as $Smo^{-/-}$ embryos established an allantoic vasculature (Astorga and Carlsson, 2007). Yet, as shown here, Smo localized to the allantois during early vasculogenesis. However, a role for Hedgehog in other aspects of allantoic vascular development, particularly patterning the nascent umbilical artery, which runs through the midline of the allantois, was not considered in that study. Midline placement of the nascent umbilical artery would seem to be critical for correct amalgamation with the dorsal aortae and vessel of confluence. Given Ptc-1's abundance in midline structures, it is possible that, while Hedgehog may be dispensable for allantoic vascularization (Astorga and Carlsson, 2007), it plays a role in positioning the nascent umbilical artery to the midline of the allantois, ensuring its correct juxtaposition to the dorsal aortae and OA. Nevertheless, it is intriguing to note that in $Smo^{-/-}$ embryos, VEGF mRNA levels were affected in the anterior, but not posterior region, including the allantois (Coultas et al., 2010). Thus, while the signals and origins of the cues that guide vasculogenesis in the allantois remain unidentified, regionalized distinctions in basic vasculogenesis in the embryo may reveal exciting alternate pathways to building a blood vessel.

CONCLUSIONS

Little is known about how the posterior region of the mammal is built. This includes the origin of most of the cell types and tissues described here and, especially, the anatomical and molecular relationship between the umbilical cord, definitive fetal body wall and gut, yolk sac and amnion. Our data revealed the presence of Hedgehog components in a large number of posterior sites, including the VCM and eventually, the DCM of the allantois, the nascent posterior arterial system, hematopoietic cells, the hindgut, and an array of ventral epithelial surfaces. In addition, they extend the role of Hedgehog to the Sinuses of Duval and the intraplacental yolk sac of the chorio-allantoic placenta. Given that a large number of umbilical defects are associated with anomalies in these tissues and developing organ systems, results here clarified the physical relationship between these components, schematized in Fig. 12.

The vessel of confluence (VOC), a poorly described arterial vessel, is a major vascular crossroads situated within the midline of the allantois. Its location undoubtedly ensures proper alignment of the posterior arterial system between the fetus and its associated extraembryonic tissues. The VOC maintains a fixed position in the posterior midline from which the umbilical artery extends posteriorly to the chorion, and the omphalomeseneteric and dorsal aortae which extend anteriorly within the embryo proper. Intriguingly, the dorsal aortae are common to all vertebrates, while the allantois and yolk sac may be later amniote adaptations to life in the egg and within the mother. The vessel of confluence may be an evolutionary response to an extreme form of viviparity to meet the demands of a rapidly growing fetus within its mother, ensuring efficient channeling of blood to the chorionic disk. In addition, maximizing the blood-forming capacity of this vessel through hematopoiesis, as demonstrated in this study, could be an additional survival strategy.

What we here call the vessel of confluence (VOC) has been designated the omphalomeseneteric artery within the 6–8-somite stage allantois (Snell and Stevens, 1966). The VOC appears to evolve into what others have described as the embryonic component of the umbilical artery, recurving posteriorly to become the left and right medial umbilical arteries associated with the paired dorsal aortae that have not yet fused, and lengthening anteriorly to become the omphalomeseneteric artery (e.g., see Fig. 2, (Gest and Carron, 2003). Thus, much confusion exists in the literature concerning the nature of the nascent posterior blood vessels and their site of confluence. Many authors have suggested that the vitelline system of arteries, which will consist of celiac, superior mesenteric, and inferior mesenteric arteries at stages later than those described here, originate from the dorsal aorta (see discussion in Gest and Carron, 2003). However, these posterior vitelline vessels seem not to have been traced back to their origin during earlier stages. Nevertheless, at least one author has suggested that “the umbilical arteries are regarded as caudal precocious members of the vitelline series” (Gest and Carron, 2003, quoted from (Dawson, 1922). Given that we have examined the posterior vasculature at earlier timepoints in this study, our data may clarify the relationship between the umbilical and omphalomeseneteric arteries, both of which might share a common origin within the vessel of confluence.

Whether the VOC is formed independently of the umbilical and omphalomeseneteric arteries in not clear, but studies in the chick have suggested that the vitelline and fetal dorsal aortae originate at distant sites and then converge in the posterior region of the fetus (reviewed in (Downs, 2003). Results from our laboratory suggested that allantoic vessels form distally, and spread proximally to the base, joining the yolk sac vessels that originated in the blood islands and spread toward the allantois, and the fetal dorsal aortae which converge on this region from the anterior end of the fetus (Downs et al., 1998).

Whatever the VOC's precise origin, we suggest that the associated Ptc-1-positive VCM may induce formation of the VOC through Hedgehog signaling, and that the VOC then forms a fixed point at which these critical posterior vessels merge. We also put forth the idea that, from the VOC, the Ptc-1-positive visceral endoderm closes with posterior-to-anterior directionality along the midline to create the omphalomeseneteric artery and hindgut tube. At the same time, the Ptc-1-positive somatopleure and splanchnopleure became continuous with the allantois at the umbilical ring which, consequent to tail turning, was incorporated into the ventral midline. Like previous findings in the anterior region, all of these posterior midline structures appear to involve Hedgehog signaling as well. Finally, in addition to its association with the posterior arterial system, Ptc-1 was found within blood cells of the intraplacental yolk sac which, as described in this study, may form as early as Phase I, ultimately becoming placental sites of hematopoiesis.

Together, these observations suggest that, like the OA and dorsal aortae, the nascent umbilical artery and vessel of confluence are hemogenic. In addition, they suggest that the intraplacental yolk sac (IPY), hitherto known only to be involved in calcium homeostasis (Bruns et al., 1985), is also hematopoietic; not only do these data place the timing of hematopoiesis in the placenta several days earlier than that previously described (Gekas et al., 2005; Otterbach and Dzierzak, 2005), but they also suggest that at least some placental hematopoietic niches reside within the IPY. Intriguingly, like Ptc-1, Runx-1 is present in the VER, suggesting coordinated roles for both gene products in deployment of stem cells from this posterior region.

The consistent relationship between Ptc-1 and hematopoietic arteries suggests that Ptc-1 may play a role in arterial specification and hematopoiesis in the posterior region, while lower levels of Ptc-1, as shown here in the sites of umbilical vein formation, may specify veins. This interpretation of our data is supported by recent studies in zebrafish which suggested that Hedgehog signaling promoted arterial specification while repressing venous cell fate (Williams et al., 2010).

In summary, given the extensive blueprint of Hedgehog signaling in the posterior region reported here, gain/loss of function experiments of the Hedgehog pathway can now be carried out to identify downstream signaling pathways involved in specific posterior processes, including posterior arterial specification, patterning, hematopoiesis and body wall closure.

EXPERIMENTAL PROCEDURES

Animal husbandry, mouse strains, dissections, staging and whole embryo culture

Care of animals was in accord with institutional guidelines. Unless otherwise indicated, standard F2 embryological material was obtained by intercrossing inbred hybrids (B6CBAF1/J) (Jackson Laboratory, Bar Harbor, ME) (Downs, 2006). Single estrous females were selected (Champlin et al., 1973) and placed with individual stud males just before the lights went off (13.00/1.00 or 21.00/9.00 lights off/lights on); copulation plugs were identified up to 12 hours later. Heterozygous *Runx-1:lacZ* (*Runx1l*$^{z/+}$) (North et al., 2002) (gift of Dr. Nancy Speck) and *Flk-1:lacZ* (Shalaby et al., 1995) mice were maintained by outcrossing heterozygous males to inbred female hybrids, above; male offspring were genotyped by ear punching and X-gal staining these overnight. Heterozygous *lacZ* reporter males were mated with non-*lacZ*-reporter B6CBAF1/J females to provide *Runx1:lacZ*$^{+/-}$ and *Flk1:lacZ*$^{+/-}$ conceptuses for localization analyses.

Ptc1:lacZ (*Ptc1*^{tm1Mps}*/J*) reporter mice (Goodrich et al., 1997) (Jackson Laboratory, Bar Harbor, ME) were maintained by crossing *Ptc1*^{tm1Mps}*/J*$^{+/-}$ heterozygous males with

Ptc1^{tm1Mps}/$J^{+/+}$ wildtype females and vice-versa (Table 3). PCR genotyping weanling ear punches (Goodrich et al., 1997) distinguished *Ptc1:lacZ*$^{+/-}$ mice from *Ptc1*^{tm1Mps}/$J^{+/+}$. Of a large number (144) of offspring, the Mendelian ratio between *Ptc1*^{tm1Mps}/$J^{+/+}$ wildtype and heterozygous *Ptc1*^{tm1Mps}/$J^{+/-}$ on this genetic background was not 1:1 (P-value = 0.0002) (Table 3). Further, the average number of litters per couple was small, and many adult *Ptc1*^{tm1Mps}/$J^{+/-}$ heterozygous animals exhibited tumors. As the inbred mice might have been undergoing "inbreeding depression", i.e., loss of reproductive fitness as inbreeding progresses (Green, 1966), we outbred *Ptc1*^{tm1Mps}/*J* onto the B6CBAF1/J inbred hybrid background, above; the new strain, called *Ptc1:lacZ*^{DOWNS} exhibited appropriate Mendelian segregation ratios, increased fertility, and larger litter sizes as early as the first generation (Tables 3, 4, and data not shown). Further, adult animals did not exhibit tumors. Localization of Ptc-1 by X-gal staining (described in the next section) (~8.0–8.5 days postcoitum, dpc) was similar in both inbred and outbred genetic backgrounds (data not shown). Except for the regenerate studies (described below), which were carried out in the inbred *Ptc1*^{tm1Mps}/*J* background, all Hedgehog component localization described in this study was carried out on conceptuses obtained by mating outbred *Ptc1:lacZ*^{DOWNS} heterozygous males with B6CBAF1/J inbred hybrid females. In this way, at least 143/252 total conceptuses (8.0–9.75 dpc) used in this study were *Ptc1:lacZ*^{Downs} heterozygotes; embryos in excess of these numbers were used in the experiments here, but were no longer entered into the Mendelian ratios.

Dissection, staging, and whole embryo culture were as previously described (Downs and Davies, 1993; Downs, 2006). For every treatment reported here, a minimum of three conceptuses was examined, and encompassed the following stages: OB, EB, LB, EHF, LHF, 1-s, 2-s, 3-s, 4-s, 5-s, 6-s, 7-s 8-s, 9-s, 10-s (~7.0–8.75 dpc), ~12–18-s (~9.0–9.25 dpc), and 23–27-s (~9.75 dpc). Three whole mount conceptus preparations were examined at 13.0 dpc to obtain a perspective on the extent to which Hedgehog signaling persisted in key sites later in development.

X-gal staining

X-gal (5-bromo-4-chloro-3-indolyl-beta-D-galactopyranoside; Sigma, B4252) staining for Ptc-1 originally used a standard protocol employed to identify *lacZ*-expressing *Rosa26*/+ donor tissue in allantois transplantation experiments (Downs and Harmann, 1997); however, it was ultimately replaced by a modification here, described in Results (Table 2). Our standard protocol consisted of 5 mM of each of the iron components, $K_3Fe(CN)_6$ and $K_4Fe(CN)_6.3H_2O$, 2mM $MgCl_2$ and 1mg/ml X-gal (stock concentration 40 mg/ml DMSO). X-gal staining on fixed conceptuses (4% paraformaldehyde, 2 hours, 4°C, followed by extensive rinsing in phosphate-buffered saline (PBS) (Downs et al., 2009)) was carried out for 13 – 17 hours (*Ptc1:lacZ*) and 12–20 hours (*Runx1:lacZ*) at 37°C. The whole mount Ptc-1 images in Fig. 5A, B, which demonstrate the shift of the allantoic VCM and DCM to posterior and anterior umbilical walls, and the 13.0 dpc conceptus in Fig. 7, which shows persistence of Ptc-1 in key placental and fetal sites, employed the standard X-gal reaction; all other Ptc-1 and Runx1 reporter localizations presented here employed 10 mM $K_4Fe(CN)_6$-$3H_2O$ (Iron Solution II, Table 2). No background staining for endogenous β-galactosidase activity was found in wildtype (non-reporter) littermates in any X-gal scenario.

Immunohistochemistry

Immunohistochemistry was carried out in whole conceptus preparations as previously described (Downs, 2008). Antibody sources and dilutions for immunohistochemistry were Ihh (Ab39634, Abcam; 1.0 mg/ml, rabbit polyclonal; 1/50 dilution); Shh (Ab19897; Abcam; 0.4 mg/ml, rabbit polyclonal; 1/100 dilution); Smo (Ab72130; Abcam; 0.5 mg/ml, rabbit

polyclonal; 1/50 dilution); and PECAM-1 (Mec13.3, 5577355, rat anti-mouse monoclonal, Pharmingen, San Jose, CA; 0.5 mg/ml; 1/100 dilution for all uncultured specimens; and PECAM-12H8, MAB1398Z, hamster anti-mouse monoclonal, formerly Chemicon, now Millipore, Billerica, MA; 0.1 mg/ml; 1/100 dilution for all cultured specimens). We also tried Desert Hedgehog (Dhh; Ab86061; Abcam; rat monoclonal, 0.5 mg/ml) at various stages (EHF to 6-s), using dilutions as low as 1/50, but no convincing signal was detected anywhere in the conceptus with this antibody; later stages were not examined. Afadin and alpha-4-integrin were used as previously described (Daane et al., 2011). All secondary antibodies were used at a dilution of 1/500 (Santa Cruz Biotechnologies: donkey anti-rabbit sc-2089; donkey anti-goat sc-2042; goat anti-rat sc-2041; goat anti-Armenian hamster sc-2445; all secondary antibodies 200 μg/0.5 ml). For IHC controls, reactions in the absence of primary antibody were used on headfold- and early somite-stage specimens in two reactions in the same experiment, ± primary antibody (Smo, Shh, and Ihh). No non-specific background staining was observed (data not shown). PECAM-1, afadin, and alpha-4-integrin controls were as previously described (Downs, 2002; Inman and Downs, 2006; Daane et al., 2011). Finally, to prevent the intensity of the X-gal precipitate from interfering with analysis of antibody localization, IHC carried out in *lacZ* reporter strains sometimes employed X-gal incubation times of 6 hours, 37°C.

Histology

X-gal and immunostained specimens were prepared for histology as previously described (Downs, 2008; Downs et al., 2009). Briefly, specimens were dehydrated through increasing ethanols, cleared in Hemo-De (Science Safety Solvents, Keller, TX), and embedded in paraffin wax, after which histological sections of thickness 6 micrometers (μm) were made and counterstained either in Nuclear Fast Red or hematoxylin, coverslipped, and examined in a compound microscope.

Creation of allantoic regenerates—Creation of allantoic regenerates was as previously described (Downs et al., 2004; Downs et al., 2009). Briefly, the allantois was aspirated through a hand-pulled glass microcapillary (I.D. 66–120 μm) via the anterior yolk sac, removing the allantois from its point of insertion into the amnion and visceral yolk sac (Downs and Harmann, 1997). Operated conceptuses were cultured alongside unoperated ones (Downs, 2006) until the chronological equivalent of 6–8-s (Downs and Gardner, 1995), prior to tailbud turning, which aided evaluation of the vasculature.

Acknowledgments

The authors thank Dr. Nancy Speck for sharing insight into candidate gene expression, Professor Christoph Viebahn, Drs. Adam Wolfe and Jerry Rhee for valuable discussions, and the March of Dimes (#1-FY06-355 and #1-FY09-511 to K.M.D.) and the National Institutes of Child Health and Development (RO1 HD042706 to K.M.D) for funding. Jacob Daane was a recipient of a Hilldale research fellowship for undergraduates.

Abbreviations

ACD	allantoic core domain
AX	allantois-associated extraembryonic visceral endoderm
DCM	dorsal cuboidal mesothelium
IPS	intraembryonic primitive streak
IPY	intraplacental yolk sac
VCM	ventral cuboidal mesothelium

VER	Ventral Ectodermal Ridge
VOC	Vessel of Confluence
XPS	extraembryonic primitive streak

References

Astorga J, Carlsson P. Hedgehog induction of murine vasculogenesis is mediated by Foxf1 and Bmp4. Development. 2007; 134:3753–3761. [PubMed: 17881493]

Bitgood MJ, McMahon AP. Hedgehog and Bmp genes are coexpressed at many diverse sites of cell-cell interaction in the mouse embryo. Dev Biol. 1995; 172:126–138. [PubMed: 7589793]

Brewer S, Williams T. Finally, a sense of closure? Animal models of human ventral wall defects. Bioessays. 2004; 26:1307–1321. [PubMed: 15551266]

Bruns ME, Kleeman E, Mils SE, Bruns DE, Herr JC. Immunochemical localization of vitamin D-dependent calcium-binding protein in mouse placenta and yolk sac. Anat Rec. 1985; 213:514–517. 532–535. [PubMed: 4083532]

Carter AM. Sources for comparative studies of placentation. I. Embryological collections. Placenta. 2007; 29:95–98. [PubMed: 17980906]

Champlin AK, Dorr DL, Gates AH. Determining the stage of the estrous cycle in the mouse by the appearance of the vagina. Biol Reprod. 1973; 8:491–494. [PubMed: 4736343]

Chang H, Li Q, Moraes RC, Lewis MT, Hamel PA. Activation of Erk by sonic hedgehog independent of canonical hedgehog signaling. Int J Biochem Cell Biol. 2010; 42:1462–1471. [PubMed: 20451654]

Chiang C, Litingtung Y, Lee E, Young KE, Corden JL, Westphal H, Beachy PA. Cyclopia and defective axial patterning in mice lacking Sonic hedgehog gene function. Nature. 1996; 383:407–413. [PubMed: 8837770]

Corbel C, Salaun J, Belo-Diabangouaya P, Dieterlen-Lievre F. Hematopoietic potential of the pre-fusion allantois. Dev Biol. 2007; 301:478–488. [PubMed: 17010964]

Cross JC. How to make a placenta: mechanisms of trophoblast cell differentiation in mice--a review. Placenta. 2005; 26(SupplA):S3–9. [PubMed: 15837063]

Cross JC, Simmons GJ, Watson ED. Chorio-allantoic morphogenesis and formation of the placental villous tree. Ann N Y Acad Sci. 2003; 995:84–93. [PubMed: 12814941]

Daane J, Enders AC, Downs KM. Mesothelium of the murine allantois exhibits distinct regional properties. J Morphology. 2011; 272:536–556.

Dannenberg, AM.; Suga, M. Histochemical stains for macrophages in cell smears and tissue sections: beta-galactosidase, acid phosphatase, nonspecific esterase, succinic dehydrogenase, and cytochrome oxidase. In: Adams, DO.; Edelson, PJ.; Koren, HS., editors. Methods for studying mononuclear phagocytes. New York, New York: Academic Press; 1981. p. 375-396.

Dawson AB. The origin and occurrence of the single umbilical artery in normal and abnormal human fetuses. Anat Rec. 1922; 24:321–349.

Downs KM. Early placentation in the mouse. Placenta. 2002; 23:116–131. [PubMed: 11945078]

Downs KM. Historical Perspective: Florence Sabin and the mechanism of blood vessel lumenization during vasculogenesis. Microcirculation. 2003; 10:5–25. [PubMed: 12610661]

Downs KM. In vitro methods for studying vascularization of the murine allantois and allantoic union with the chorion. Methods Mol Med. 2006; 121:241–272. [PubMed: 16251748]

Downs KM. Systematic localization of Oct-3/4 to the gastrulating mouse conceptus suggests manifold roles in mammalian development. Dev Dyn. 2008; 237:464–475. [PubMed: 18213575]

Downs KM, Davies T. Staging of gastrulation in mouse embryos by morphological landmarks in the dissection microscope. Development. 1993; 118:1255–1266. [PubMed: 8269852]

Downs KM, Gardner RL. An investigation into early placental ontogeny: allantoic attachment to the chorion is selective and developmentally regulated. Development. 1995; 121:407–416. [PubMed: 7768182]

Downs KM, Gifford S, Blahnik M, Gardner RL. The murine allantois undergoes vasculogenesis that is not accompanied by erythropoiesis. Development. 1998; 125:4507–4521. [PubMed: 9778509]

Downs KM, Harmann C. Developmental potency of the murine allantois. Development. 1997; 124:2769–2780. [PubMed: 9226448]

Downs KM, Hellman ER, McHugh J, Barrickman K, Inman K. Investigation into a role for the primitive streak in development of the murine allantois. Development. 2004; 131:37–55. [PubMed: 14645124]

Downs KM, Inman KE, Jin DX, Enders AC. The Allantoic Core Domain (ACD): New insights into development of the murine allantois and its relation to the primitive streak. Dev Dyn. 2009; 238:532–553. [PubMed: 19191225]

Duval, M. Le placenta des rongeurs. In: Alcan, F., editor. Extrait du journal de l'anatomie et de la physiologie annees 1889–1892. Paris: Ancienne Librarie Gemner Bailliere; 1892.

Epstein DJ, McMahon AP, Joyner AL. Regionalizaiton of Sonic hedgehog transcription along the anteroposterior axis of the mouse central nervous system is regulated by Hnf3-dependent and -independent mechanisms. Development. 1999; 126:281–292. [PubMed: 9847242]

Garcia-Porrero JA, Godin IE, Dieterlen-Lievre F. Potential intraembryonic hemogenic sites at pre-liver stages in the mouse. Anat Embryol. 1995; 192:425–435. [PubMed: 8546334]

Gekas C, Dieterlen-Lievre F, Orkin SH, Mikkola HKA. The placenta is a niche for hematopoietic stem cells. Dev Cell. 2005; 8:365–375. [PubMed: 15737932]

Gest TR, Carron MA. Embryonic origin of the caudal mesenteric artery in the mouse. Anat Rec. 2003; 271:192–201.

Goodrich LV, Johnson RL, Milenkovic L, McMahon JA, Scott MP. Conservation of the hedgehog/patched signaling pathway from flies to mice: induction of a mouse patched gene by Hedgehog. Genes Dev. 1995; 10:301–312. [PubMed: 8595881]

Goodrich LV, Milenkovic L, Higgins KM, Scott MP. Altered neural cell fates and medulloblastoma in mouse patched mutants. Science. 1997; 277:1109–1113. [PubMed: 9262482]

Green, EL. Breeding systems. The Laboratory Mouse; 1966.

Holt, SJ.; Sadler, PW. Studies in enzyme cytochemistry III. Relationships between solutbility, molecular association and structure in indigoid dyes; Proc Royal Soc(London). 1958. p. 495http://rarediseases.info.nih.gov/

Inman KE, Downs KM. Brachyury is required for elongation and vasculogenesis in the murine allantois. Development. 2006; 133:2947–2959. [PubMed: 16835439]

Inman KE, Downs KM. The murine allantois: emerging paradigms in formation and development of the mammalian umbilical cord and its relation to the fetus. genesis. 2007; 45:237–258. [PubMed: 17440924]

Jenkins D. Hedgehog signalling: emerging evidence for non-canonical pathways. Cell Signal. 2009; 21:1023–1034. [PubMed: 19399989]

Jiang G, Herman GE. Analysis of Nsdhl-deficient embryos reveals a role for Hedgehog signaling in early placental development. Hum Mol Genet. 2006; 15:3293–3305. [PubMed: 17028112]

Lojda Z. Indigogenic methods for glycosidases. Histochimie. 1970; 22:3.

Matsumaru D, Haraguchi R, Miyagawa S, Motoyama J, Nakagata N, Meijlink F, Yamada G. Genetic analysis of hedgehog signaling in ventral body wall development and the onset of omphalocele formation. PLos One. 2011; 6:e16260. [PubMed: 21283718]

Motoyama J, Takabatake T, Takeshima T, Hui C-C. Ptch2, a second mouse Patched gene is co-expressed with Sonic Hedgehog. Nature Genet. 1998; 18:104–106. [PubMed: 9462734]

Naiche LA, Papaioannou VE. Loss of *Tbx4* blocks hindlimb development and affects vascularization and fusion of the allantois. Development. 2003; 130:2681–2693. [PubMed: 12736212]

Newman PJ. The biology of PECAM-1. J Clin Invest. 1997; 99:3–8. [PubMed: 9011572]

Newman PJ, Newman DK. Signal transduction pathways mediated by PECAM-1: new roles for an old molecule in platelet and vascular cell biology. Arterioscler Thromb Vasc Biol. 2003; 23:953–964. [PubMed: 12689916]

North TE, deBruijn MF, Stacy T, Talebian L, Lind E, Robin C, Binder M, Dzierzak E, Speck NA. Runx1 expression marks long-term repopulating hematopoietic stem cells in the midgestation mouse embryo. Immunity. 2002; 16:661–672. [PubMed: 12049718]

North TE, Gu T-L, Stacy T, Wang Q, Howard L, Binder M, Marin-Padilla M, Speck NA. Cbfa2 is required for the formation of intra-aortic hematopoietic clusters. Development. 1999; 126:2563–2575. [PubMed: 10226014]

Otterbach K, Dzierzak E. The murine placenta contains hematopoietic stem cells within the vascular labyrinth region. Dev Cell. 2005; 8:377–387. [PubMed: 15737933]

Peeters M, Ottersbach K, Bollerot K, Orelio C, deBruijn M, Wijgerde M, Dzierzak E. Ventral embryonic tissues and Hedgehog proteins induce early AGM hematopoietic stem cell development. Development. 2009; 136:13–21.

Poulsen LK, Dalton HM, Angles ML, Marshall KC, Molin S, Goodman AE. Simultaneous determination of gene expression and bacterial identity in single cells in defined mixtures of pure cultures. Appl Environ Microbiol. 1997; 63:3698–3702. [PubMed: 9293021]

Roessler E, Belloni E, Gaudenz K, Jay P, Berta P, Scherer SW, Tsui LC, Muenke M. Mutations in the human Sonic Hedgehog gene cause holoprosencephaly. Nat Genet. 1996; 14:357–360. [PubMed: 8896572]

Rossant J, Cross JC. Placental development: lessons from mouse mutants. Nat Rev Genet. 2001; 2:538–548. [PubMed: 11433360]

Shalaby F, Rossant J, Yamaguchi TP, Gertsenstein M, Wu X-F, Breitman ML, Schuh AC. Failure of blood-island formation and vasculogenesis in Flk-1 deficient mice. Nature. 1995; 376:62–66. [PubMed: 7596435]

Snell, GB.; Stevens, LC. Early embryology. In: Green, EL., editor. Biology of the Laboratory Mouse. New York: McGraw Hill; 1966. p. 205-245.

Stevenson, RE.; Hall, JG., editors. Human malformations and related anomalies. Oxford: Oxford University Press; 2006.

Swiers G, deBruijn M, Speck NA. Hematopoietic stem cell emergence in the conceptus and the role of Runx1. Int J Dev Biol. 2010; 54:1151–1163. [PubMed: 20711992]

Takabatake T, Ogawa M, Takahashi TC, Mizuno M, Okamoto M, Takeshima K. Hedgehog and patched gene expression in adult ocular tissues. FEBS Lett. 1997; 410:485–489. [PubMed: 9237688]

Trempus CS, Morris RJ, Bortner CD, Cotsarelis G, Faircloth RS, reece JM, Tennant RW. Enrichment for living murine karatinocytes from the hair follicle bulge with the cell surface marker CD34. J Invest Dermatol. 2003; 120:501–511. [PubMed: 12648211]

Walls JR, Coultras L, Rossant J, Henkelman RM. Three-dimensional analysis of vascular development in the mouse embryo. PLoS One. 2008; 3:e2843. [PubMed: 18665227]

Williams C, Kim S-H, Ni TT, Mitchell L, Ro H, Penn JS, Baldwin SH, Solnica-Krezel L, Zhong TP. Hedgehog signaling induces arterial endothelial cell formation by repressing venous cell fate. Dev Biol. 2010; 341:196–204. [PubMed: 20193674]

Wilson CW, Chuang PT. Mechanism and evolution of cytosolic Hedgehog signal transduction. Development. 2010; 137:2079–2094. [PubMed: 20530542]

Yamaguchi TP, Dumont DJ, Conlon RA, Breitman ML, Rossant J. flk-1, an flt-related receptor tyrosine kinase, is an early marker for endothelial cell precursors. Development. 1993; 118:488–498.

Yokomizo T, Dzierzak E. Three-dimensional cartography of hematopoietic clusters in the vasculature of whole mouse embryos. Development. 2010; 137:3651–3661. [PubMed: 20876651]

Zeigler BM, Sugiyama D, Chen M, Guo Y, Downs KM, Speck NA. The allantois and chorion, which are isolated before circulation or chorio-allantoic fusion, have hematopoietic potential. Development. 2006; 133:4183–4192. [PubMed: 17038514]

Zovein AC, Turlo KA, Ponec RM, Lynch MR, Chen KC, Hofmann JJ, Cox TC, Gasson JC, Iruela-Arispe ML. Vascular remodeling of the vitelline artery initiates extravascular emergence of hematopoietic clusters. Blood. 2010; 116:3435–3544. [PubMed: 20699440]

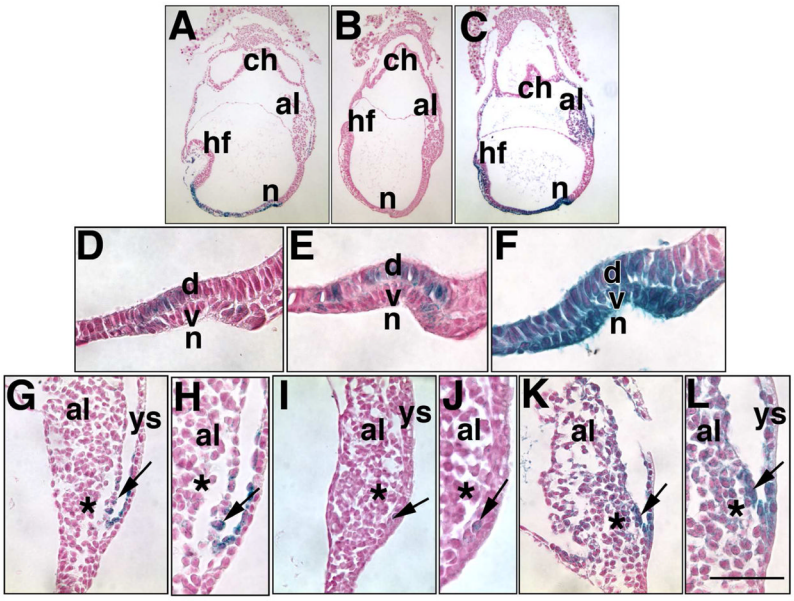

Fig. 1. Comparison of X-gal staining methods to visualize Ptc-1 in the allantois and node

Ptc1:lacZ heterozygotes were stained at the Early Headfold (EHF) stage in the following concentrations of iron-containing potassium reagents, in which 2 mM $MgCl_2$, 1 mg/ml X-gal and 37°C were kept constant: (**A, D, G, H**) Standard protocol, 5mM $K_3Fe(CN)_6$, 5mM $K_4Fe(CN)_6.3H_2O$; note that X-gal staining is found at low levels in both ventral (v) and dorsal (d) components of the node (n) (D), and in the VCM (arrow, G, H), but barely perceptible in the ACD (asterisk G, H). (**B, E, I, J**) 10mM 5mM $K_3Fe(CN)_6$; note that, while X-gal is visible in both components of the node (E), it is detectable in only a few cells of the VCM (arrows, I, J) and not in the ACD (asterisks, I, J). (**C, F, K, L**) 10 mM $K_4Fe(CN)_6$-$3H_2O$; note that X-gal is robust in both components of the node (F), the VCM and adjacent visceral components of the yolk sac, both mesodermal and endodermal, and within the allantoic core domain (asterisk). After sectioning, specimens were dewaxed and counterstained in Nuclear Fast Red. Scale bar (L): Other abbreviations: al, allantois; ch, chorion; hf, headfolds. Scale bar (L): 50 μm (D–F, H, J, L); 25 μm (G, I, K); 112 μm (A–C). All scale bar lengths are approximate to within 25 μm in this and all subsequent Figures.

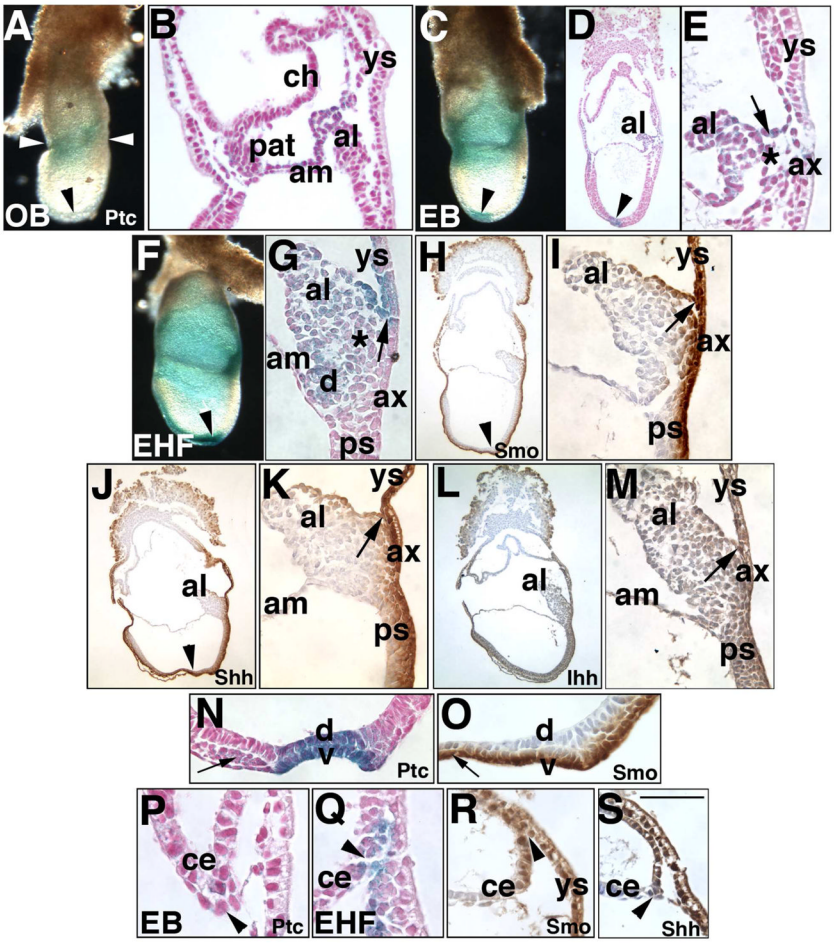

Fig. 2. Localization of hedgehog signaling components: Phase I (Neural plate/no allantoic bud (OB)- Headfold (HF) stages, ~7.0–8.0 dpc)

In this and all figures, stages are indicated in the lower left; unstaged panels correspond to the last indicated stage. All orientations are sagittal, with anterior on the left, and posterior on the right. In this and all figures, the proteins analyzed are indicated in the lower right of panels; unlabeled panels correspond to the last indicated gene product. (**A, B**) Neural plate/ No allantoic bud (OB) stage (~7.0 dpc), Ptc-1 (royal blue color). Whole mount (A) and sectioned (B) specimens. Arrowhead (A) indicates the node, which, at this stage, does not exhibit perceptible Ptc-1 when examined in section (also compare this whole mount specimen with the node in panel C, arrowhead). White arrowheads bracket the Ptc-1-positive embryonic/extraembryonic junction that is enlarged in B. al, allantois; am, amnion; ch, chorion, pat, proamniotic tube; ys, visceral yolk sac. (**C–E**) Neural plate/Early bud (EB) stage (~7.25 dpc), Ptc-1. Whole mount (C) and sectioned (D, E) specimens. Note the presence of Ptc-1 in the node (arrowheads, C, D); arrow (E) indicates Ptc-1-positive presumptive VCM on the allantois (al); asterisk (E) indicates the allantoic core domain (ACD). (**F, G**), Early headfold (EHF) stage (~7.75 dpc), Ptc-1. Whole mount (F) and sectioned (G) specimens. Placement of the arrow (G) indicates the VCM and its association with the visceral yolk sac; asterisk indicates the ACD. d, dorsal cuboidal mesothelium (DCM, see text). Note the low-level of Ptc-1 in the allantois-associated extraembryonic visceral endoderm (ax). (**H, I**) EHF stage, Smoothened (Smo), sectioned specimen. Note in (H) that Smo is found throughout the visceral endoderm, both embryonic and extraembryonic, and associated underlying cells, several layers thick, as well as in the

ventral node (arrowhead, H) and notochord and VCM of the allantois, seen at higher magnification in (I) (arrow). (**J, K**) EHF stage, Sonic hedgehog (Shh) IHC, sectioned specimen. Note in (J) that, like Smo, Shh localizes to the visceral endoderm, both embryonic and extraembryonic, and several underlying cell layers, as well as to the ventral node (arrowhead, J) and notochord, and VCM of the allantois, seen at higher magnification in (K), arrow, at its intersection with the visceral yolk sac (ys). (**L, M**) EHF stage, Indian hedgehog (Ihh) sectioned specimen. Comparison of Ihh with Smo and Shh reveals that Ihh is less intense in the visceral endoderm and VCM (arrow, M). (**N, O**) EHF stage, Ptc-1 (N) is found in both dorsal (d) and ventral (v) layers of the node; for reasons that are unclear, Smo (O) localizes to the ventral layer only. The small arrows in each panel indicate the notochord. (**P–S**) Series of sections of presumptive intraplacental yolk sac in the chorionic ectoderm (ce) and visceral yolk sac (ys). Arrowheads indicate Ptc-1 (arrowheads, P, Q), Smo (arrowhead, R), and Shh (arrowhead, S) in this region. Scale bar (S): 50 μm (E, G, P-R); 35 μm (I, K, M-O, S); 140 μm (H, J, L); 100 μm (B, D); 400 μm (A, C, F).

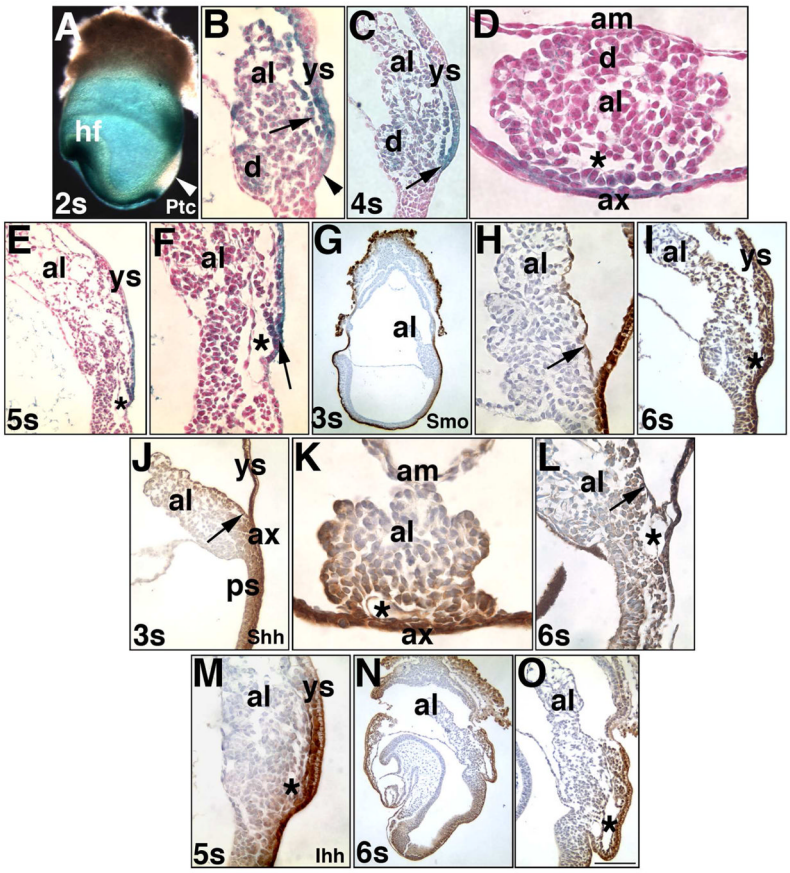

Fig. 3. Localization of Hedgehog signaling components: Phase II (1–9-s; ~8.0–8.75 dpc)

With the exception of the transverse orientations in (D, K), all other orientations are sagittal, with anterior on the left, and posterior on the right. Only the specimen in (A) is a whole mount preparation; the others have been sectioned. (**A, B**) 2-s stage (~8.25 dpc), Ptc-1. White arrowhead (A) indicates the primitive streak, which does not exhibit detectable Ptc-1 in the *Ptc1:lacZ* reporter. Arrow (B) indicates the Ptc-1-positive VCM; the DCM (d) opposite is also Ptc-1 positive; the allantois-associated extraembryonic visceral endoderm (ax) now clearly contains Ptc-1 (arrowhead). (**C, D**) 4-s stage (~8.5 dpc), Ptc-1. Arrow (C) indicates the intersection between the VCM and adjacent visceral yolk sac (ys); the symmetrically opposite DCM (d) is modestly Ptc-1. The relationship between the VCM and allantois-associated extraembryonic visceral endoderm (ax) are observed in transverse orientation; the asterisk indicates the vessel of confluence (VOC) forming beneath the VCM; the DCM (d) is opposite. (**E, F**) 5-s stage (~8.5 dpc), Ptc-1. Overview of the allantois (E); proximal allantois (F) shows the Ptc-1-positive VCM (arrow) overlying the vessel of confluence, VOC (asterisk) at its intersection with the Ptc-1-positive visceral yolk sac (ys), and just above the hindgut invagination. (**G, H**) 3-s stage (~8.25 dpc), Smo. Smo is in the visceral endoderm that surrounds most of the egg cylinder and in the allantoic VCM (H, arrow). (I) 6-s stage (~8.5 dpc), Smo. Smo localizes to the VCM overlying the vessel of confluence, VOC (asterisk) and ventral surface of the allantois, adjacent to the Smo-positive yolk sac (ys). (**J, K**) 3-s stage, Shh. Shh penetrates several cell layers, clearly shown in transverse section of the allantois (K), where the VOC (asterisk) is forming. (**L**) 6-s stage, Shh. The Shh-positive VCM (arrow) overlies the VOC (asterisk). (**M**) 5-s stage, Ihh. Ihh is found in the VCM, associated visceral yolk sac (ys), and VOC (asterisk). As with Shh, Ihh penetrates several cell layers into the conceptus. (**N, O**) 6-s stage, Ihh. The VOC (asterisk)

may be slightly positive (O). Scale bar (O): 100 μm (E, I, O); 87 μm (D, K); 50 μm (F, H, L, M); 33 μm (B); 400 μm (A); 200 μm (G, N); 150 μm (C, J).

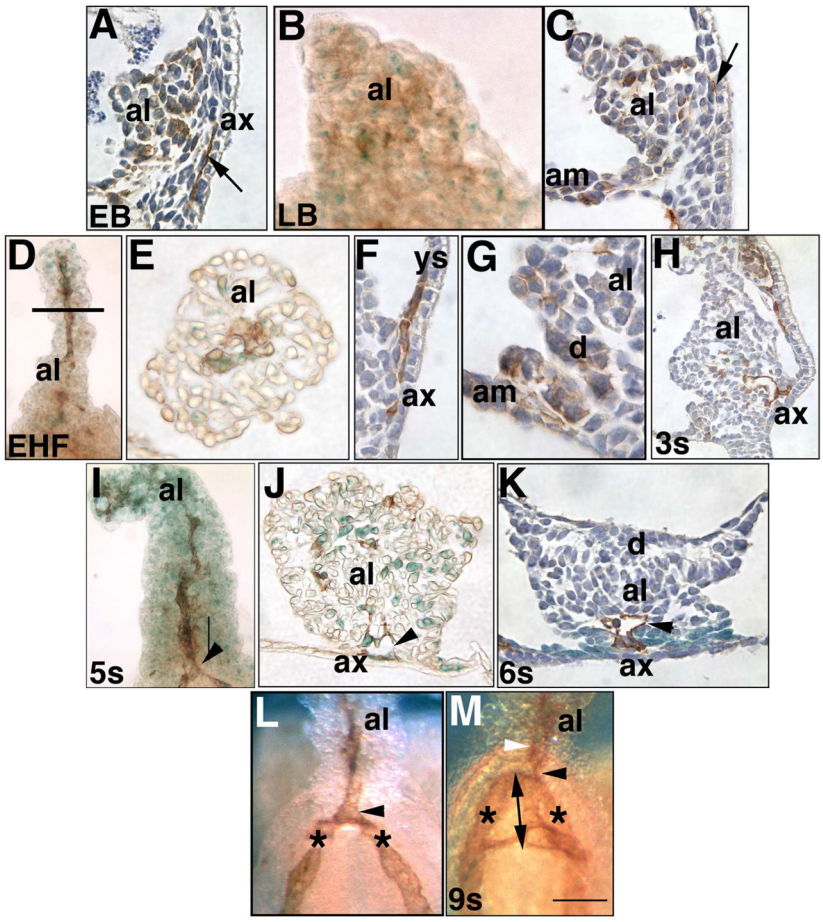

Fig. 4. Identification of posterior vascular elements (EB - 9-s; ~7.25–8.75 dpc)

PECAM-1 (brown color, counterstained with hematoxylin, dark blue color) and Flk-1 (royal blue color) in whole mount preparations of allantoises (frontal views: B, D, I, L, M) and sections (sagittal views: A, C, F, G, H; transverse views: E, J, K). (**A**) EB stage (~7.25 dpc). PECAM-1 is scattered throughout the allantoic bud (al), in both inner core and outer mesothelial cells. Arrow points to file of PECAM-1-positive cells beneath the allantois-associated extraembryonic visceral endoderm (ax). (**B**) LB stage (~7.5 dpc). PECAM-1 and Flk-1 are scattered throughout the allantois, and exhibit no patterning. (**C**) LB stage. PECAM-1 is scattered throughout the allantois. Arrow points to PECAM-1 cells immediately internal to the ax. (**D–G**) EHF stage. The allantois exhibits a midline file of PECAM-1-positive cells (D) which, as shown in transverse histological section at the approximate level indicated by the horizontal line (E) are also Flk-1-positive. PECAM-1 also localized to the site of insertion of the allantois into the yolk sac (F), where the vessel of confluence will appear beneath the vertex of the “V” formed by the VCM and its association with the visceral yolk sac (ys). Although not evident here, adjacent sections exhibited continuity with the PECAM-1-positive nascent umbilical artery. PECAM-1 was also scattered in Dorsal Cuboidal Mesothelium (d) (G). (**H**) 3-s stage (~8.25 dpc). PECAM-1-positive cells between the ax extend into the allantois, contributing to the nascent allantoic midline artery. (**I, J**) 5-s stage (~8.5 dpc). The PECAM-1-positive nascent umbilical artery has fused with the paired dorsal aortae and yolk sac vasculature at the VOC (arrowhead); the visceral yolk sac has been peeled away to reveal the allantois. Flk-1 has become abundant throughout the length of the allantois and co-localizes with PECAM-1 (J) at the vessel of

confluence, VOC (arrowhead), but is found independent of PECAM-1 in many allantoic cells. (**K**) 6-s stage (~8.5 dpc). PECAM-1-positive vessel of confluence, VOC (arrowhead) lies within a Ptc-1-positive (royal blue color) domain that encompasses the allantoic VCM. (L) 6-s stage. Vessel of confluence, VOC (arrowhead); paired dorsal aortae (asterisks). (**M**) 9-s stage (~8.75 dpc). While the allantoic artery (white arrowhead) maintains its fixed position within the base of the allantois, the double-arrow indicates what appears to be lengthening of the vessel of confluence, VOC (black arrowhead) into the embryonic region to become the omphalomeseneteric artery (double arrowhead). Note the connections at right angles between the omphalomeseneteric artery and paired dorsal aortae. Scale bar (M): Other abbreviations: am, amnion. Scale bar (M): 50 μm (H-K); 75 μm (A, C, E, F, M); 100 μm (B, D, G, L).

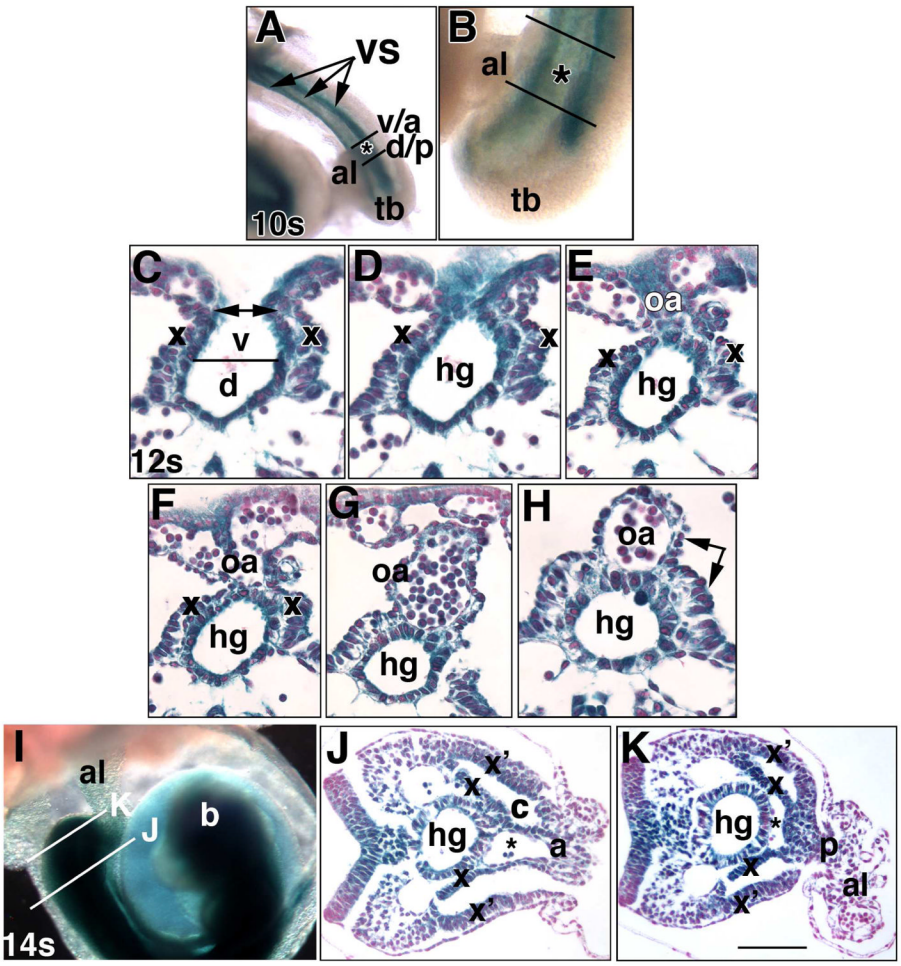

Fig. 5. Ptc-1 in the developing hindgut and omphalomeseneteric artery, proximal walls of the allantois, and the umbilical ring (Phase IIIa, ~8.75–9.25 dpc)

Specimens in all panels were prepared from the *Ptc1:lacZ* reporter mouse. Whole mount (A, B, I) and sectional (C-H, J, K) views. (**A, B**) 10-s stage (~8.75 dpc). Ventral views indicate the allantoic insertion into the ventral surface (VS, arrows, A, composed of the splanchno- and somatopleure). Black lines bracket the allantois (al) at the nascent umbilical ring; v/a: border of the insertion (asterisk) of the VCM/anterior umbilical wall into the VS; d/p: border of the insertion of the DCM/posterior umbilical wall into the VS. tb, tailbud. (**C–H**) Sequence of closure (C, double arrow) of the definitive endoderm (parsed into dorsal (d) and ventral (v) components, C) to form the hindgut (hg) tube (D–H) and omphalomeseneteric artery (oa) (E-H). x, splanchnopleure (C–I), double arrow, H, the splanchnopleure surrounds both the hindgut and OA. (**I–K**) 14-s stage (~9.25 dpc). The histological views displayed in J, K are indicated in (I) by white lines. b, developing brain. In J, K: x, splanchnopleure covering the hindgut; x', lateral somatopleure. Together, x and x' delineate the coelom (c). The vessel of confluence (asterisk) is continuous with the umbilical artery (J) at the level of VCM/anterior umbilical wall (a), and with the dorsal aortae (K) at the level of the DCM/posterior umbilical wall (p). Scale bar (K): 100 μm (J, K); 50 μm (C-H); 170 μm (B); 333 μm (I).

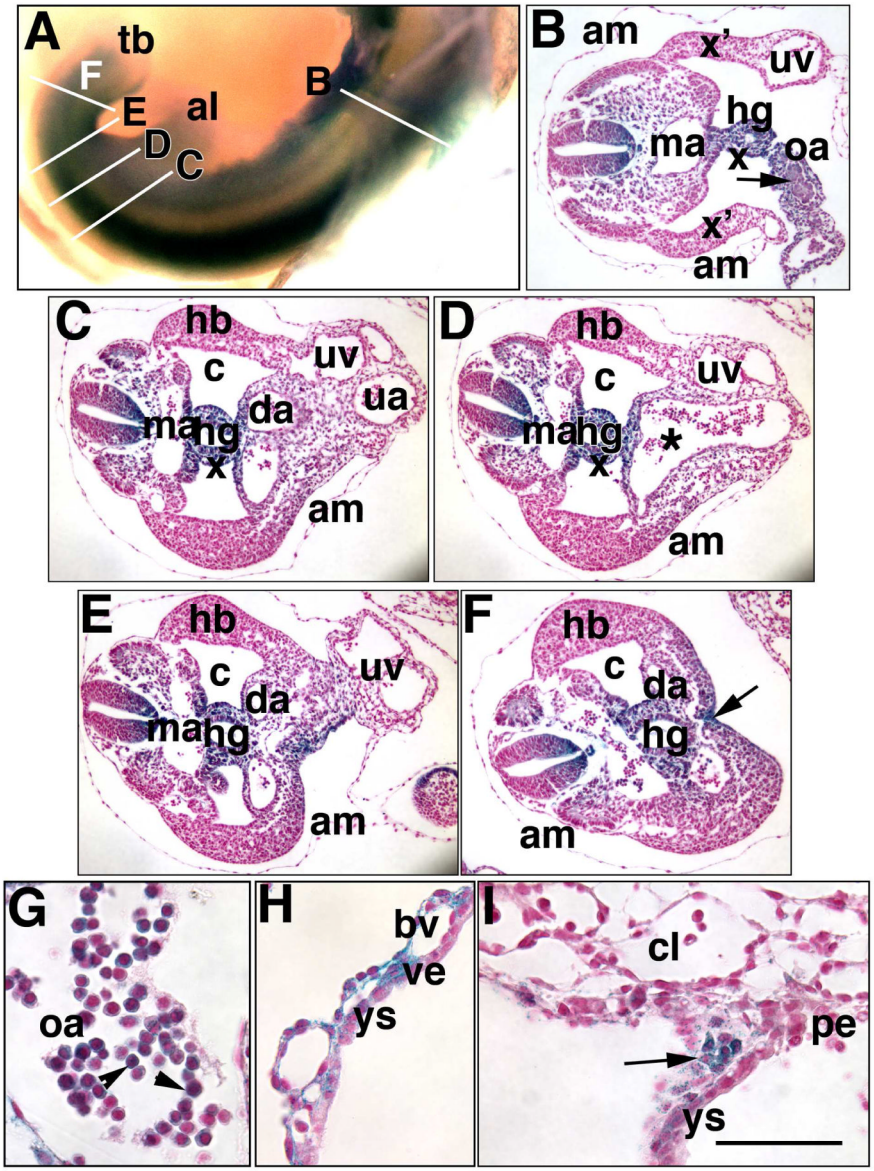

Fig. 6. Persistence of Ptc-1 in midline posterior and hematopoietic sites (Phase IIIb, 23–27-s; ~9.75 dpc)

Specimens in all panels were prepared from the *Ptc1:lacZ* reporter mouse. Whole mount (A) and sectioned specimens (B–I), the latter of which are from a single conceptus. (A) 23–27-s stage. Whole mount specimen shows white lines indicating the general level of the sections in B-F. (**B**) Section through the omphalomeseneteric artery (oa) which, at this site, forms a loose connection between the hindgut (hg) and visceral yolk sac (not shown). Ptc-1 is found in clusters of presumptive hematopoietic cells (arrow) within the oa. am, amnion; ma, midline aorta; uv, right umbilical vein; x, splanchnopleure; x', lateral somatopleure. (**C**) Section at the level of the anterior umbilical ring. c, coelom; da, distal recurved portion of the paired dorsal aortae; ua, umbilical artery; uv, umbilical vein; am, amnion. (**D**) Section through the mid-umbilical ring. Asterisk indicates the vessel of confluence and its continuation with the umbilical artery. (**E**) Section at the level of the posterior umbilical ring. (**F**) Section posterior to the posterior umbilical ring. The arrow indicates the VER. (G) Ptc-1-positive hematopoietic cells (arrowheads) found within the omphalomeseneteric artery

of this specimen. (H) Ptc-1-positive visceral yolk sac (ys) blood vessels (bv) and occasional visceral endoderm (ve). (**I**) Ptc-1-postive wall of the IPY that is in the process of forming (arrowhead) at the edges of the chorionic labyrinth (cl), visceral yolk sac (ys), and parietal endoderm (pe). Scale bar (I): 100 μm (B–F); 650 μm (A); 150 μm (H, I); 50 μm (G).

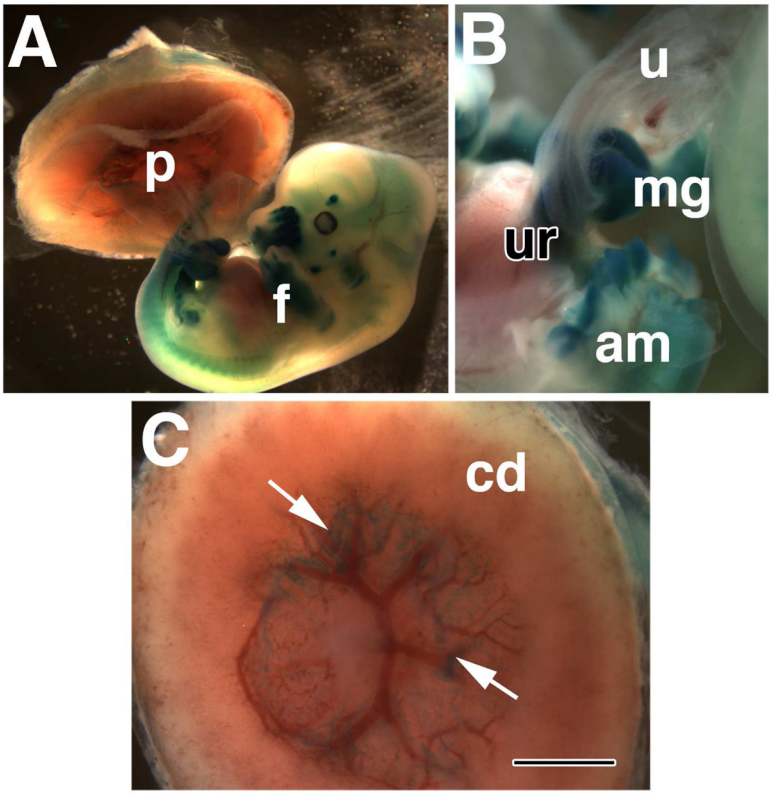

Fig. 7. Ptc-1 persists in the umbilical ring (~13.0 dpc)

Whole mount specimen from the *Ptc1:lacZ* reporter mouse strain. (**A**) Whole conceptus showing both the chorio-allantoic placenta (p) and fetus (f). (**B**) The region of the umbilical ring (ur), shows Ptc-1 in the base of the umbilical cord (u) and midgut (mg), with which the umbilicus is associated. The amnion (am) has been opened but remains connected to this site. (**C**) The fetal side of the chorionic disk (cd) of the chorio-allantoic placenta; arrows indicate Ptc-1-positive lateral regions at the points of insertion between the chorion, allantois, visceral yolk sac, and parietal endoderm. Scale bar (C): 1 mm (B, C); 3 mm (A).

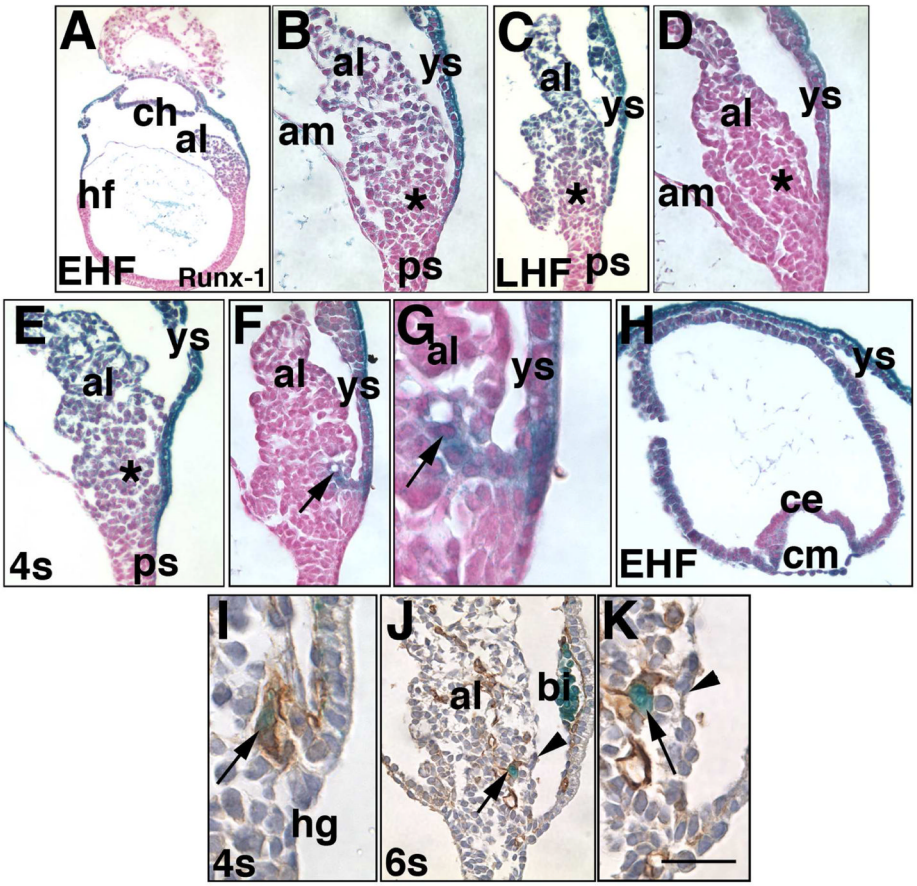

Fig. 8. Runx-1 localizes to many sites of Ptc-1 expression (EHF-6-s; ~7.75–8.5 dpc)

Histological sections from the *Runx1:lacZ* reporter mouse conceptus (A-K), and co-stained for PECAM-1 (I–K). X-gal staining: 6 hours (I-K), 12 hours (D, F-H), 20 hours (A–C, E). (**A, B**) EHF stage (~7.75 dpc), whole conceptus (A) and allantois (al) (B) showing Runx-1 throughout the allantois, especially in more distal regions, and in the visceral yolk sac (ys), both visceral endoderm and mesodermal components. Asterisk in (B) and in subsequent panels (C–E, M) indicates the approximate site of the allantoic core domain (ACD). (**C, D**) LHF stage (~8.0 dpc), 20- (C) and 12- (D) hour X-gal staining shows that the most Runx-1-abundant sites are the visceral yolk sac (ys) and distal region of the allantois. (**E–G**) 4-s stage (~8.5 dpc). 20- (E) and 12- (F, G) hour X-gal staining reveals that the visceral yolk sac (ys), distal allantoic region, and VCM and vessel of confluence (arrows, F, G) express the highest levels of Runx-1. (H) EHF stage, chorion. While the chorionic mesoderm (cm) is Runx-1-positive throughout, chorionic ectoderm (ce) is most intensely Runx-1 in the more lateral regions. (**I**) 4-s stage. Runx-1/PECAM-1 are found in the emergent vessel of confluence (arrow), which is continuous with the unbranched portion of the nascent allantoic artery, though not seen here. (**J, K**) 6-s stage, Runx-1/PECAM-1 shows a Runx-1-positive cell (arrows, J, K) within the PECAM-1-positive nascent umbilical artery, which lies just beneath the VCM (arrowheads). Note the Runx-1-positive cells in the yolk sac blood islands (bi) (J). Scale bar (K): 50 μm (B, D, F, J,); 75 μm (C, E, H); 125 μm (K); 150 μm (A, G, I).

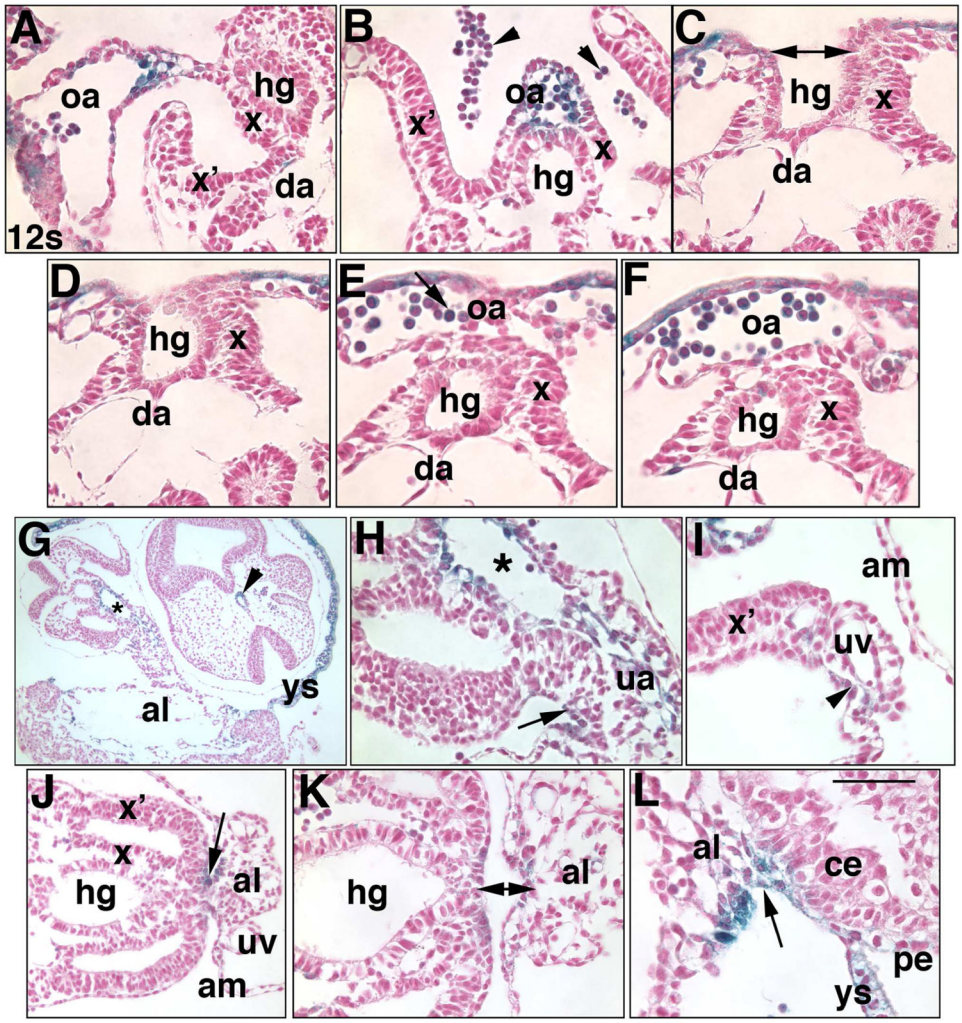

Fig. 9. Runx-1 in major posterior blood vessels (12-s, ~9.0 dpc)

All panels show histological sections from several different specimens of a *Runx1:lacZ* reporter mouse conceptus at the 12-s stage showing sites of Runx-1 (royal blue color, counterstained with Nuclear Fast Red). (**A, B**) Runx-1 cells appear to be budding from Runx-1-positive endothelium (arrow, A) of the omphalomeseneteric artery (oa) as it forms, and in the omphalomeseneteric artery at a more posterior site (B). Arrowheads in B indicate hematopoietic cells that were liberated from their vessels during histological processing. x, splanchnopleure covering the lateral hindgut and oa; da, dorsal aortae. (**C–F**) Sequence of hindgut (hg) and omphalomeseneteric artery (oa) formation (hg, double arrowhead, C). Runx-1 is found in most cells of the visceral endoderm of the visceral yolk sac, and hematopoietic cells. (**G, H**) Runx-1-positive vessel of confluence (asterisks, G, H) and its continuity with the umbilical artery (ua, H) at the level of the mid-umbilical ring. The arrow in H indicates the former VCM, now the anterior wall of the umbilical cord, which contains Runx-1, at its site of insertion into the ventral surface. (**I**) Example of modest Runx-1 (arrowhead) in the region around the umbilical vein (uv). x', lateral somatopleure; am, amnion. (**J, K**) The arrow indicates the former DCM, now the posterior wall of the umbilical cord, which contains Runx-1, at its site of insertion into the ventral surface. The double arrow (K) shows Runx-1 at the level of the DCM/posterior umbilical wall of the allantois.

(L) Runx-1 in the presumptive intraplacental yolk sac (arrow). Scale bar (L): 50 μm (A–F; H, K, L); 100 μm (J); 200 μm (G); 12.5 μm (I).

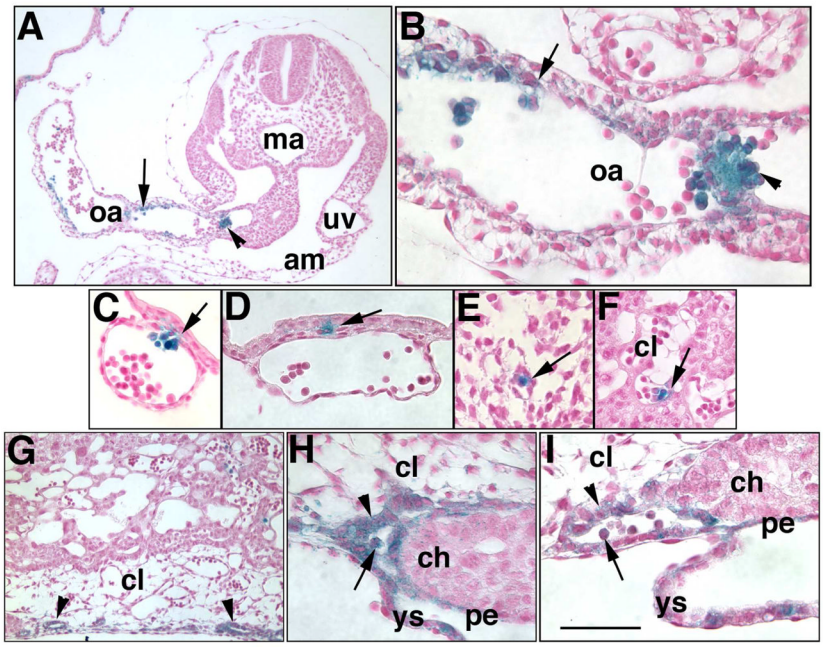

Fig. 10. Runx-1 in major posterior blood vessels (23–27-s, ~9.75 dpc)

All panels show histological sections from a single specimen of a *Runx1:lacZ* reporter mouse conceptus at the 23–27-s stage showing sites of Runx-1 (royal blue color, counterstained with Nuclear Fast Red). (**A, B**) Runx-1 in the endothelium (arrows) and hematopoietic cells (arrowheads) of the omphalomeseneteric artery (oa). (**C, D**) Runx-1 in patchy regions that appear to be part of both the visceral endoderm and mesoderm of the visceral yolk sac (arrows). (**E**) Runx-1-positive cell within loose mesoderm of the body wall. (**F**) Runx-1-positive cell within a blood vessel of the chorionic labyrinth. (**G–I**) The intraplacental yolk sac (arrowheads, G) contains Runx-1-positive endoderm (arrowheads, H), I and Runx-1-positive hematopoietic cells (arrows, **H**, I). Scale bar (I): 50 μm (C, D, F, I); 75 μm (E, H); 100 μm (B, G); 125 μm (A).

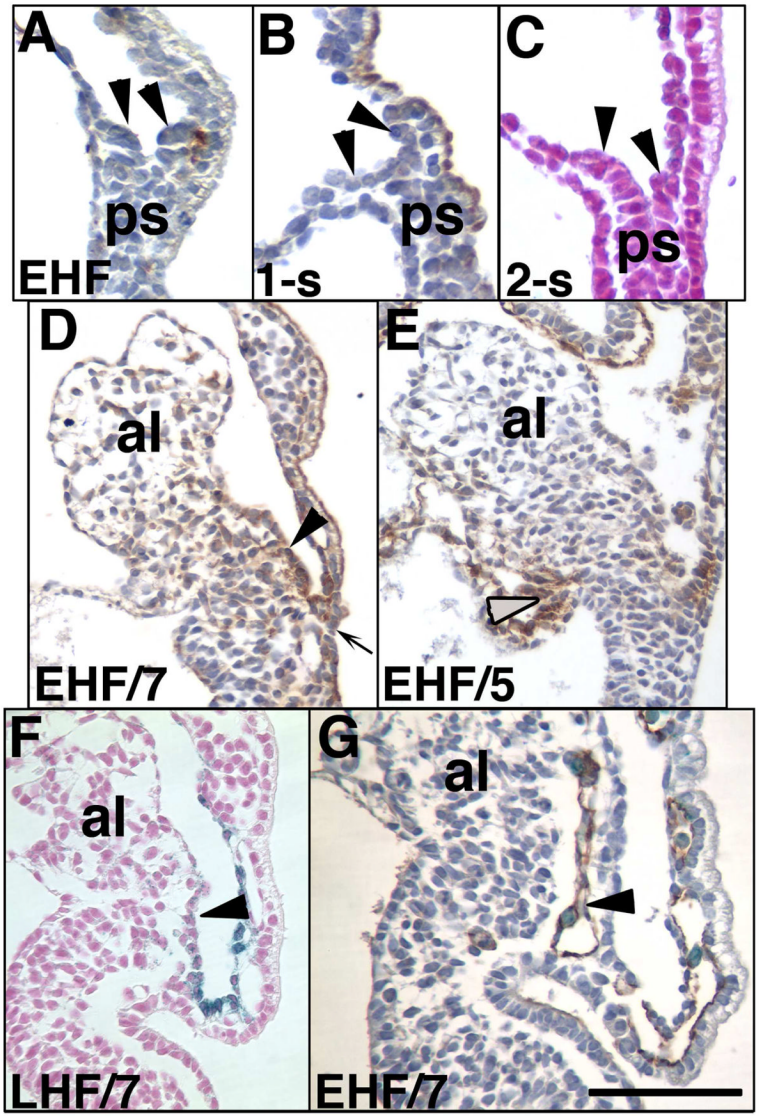

Fig. 11. Re-establishment of the VCM, DCM and hemogenic nascent umbilical artery in allantoic regenerates

(**A–C**) Allantoises were aspirated at EHF-2-s stages (~7.75–8.25 dpc) and immunostained with PECAM-1 (A), afadin (B), or X-gal in the *Ptc1:lacZ* reporter embryo (C). Arrowheads (A-C) suggest that the primitive streak (ps) may be composed of dorsal (left) and ventral (right) components. (**D–G**) Initial/final stages, lower left, allantoic regenerates. Afadin-stained VCM (arrowhead, **D**), alpha-4-integrin-stained DCM (grey arrowhead, **E**), Ptc-1 in the VCM (arrowhead, **F**); PECAM-1 (brown)/Runx-1 (royal blue) (arrowhead, **H**) in the nascent hemogenic vessel of confluence/umbilical artery. Scale bar (G): 50μm (G); 200μm (A–F).

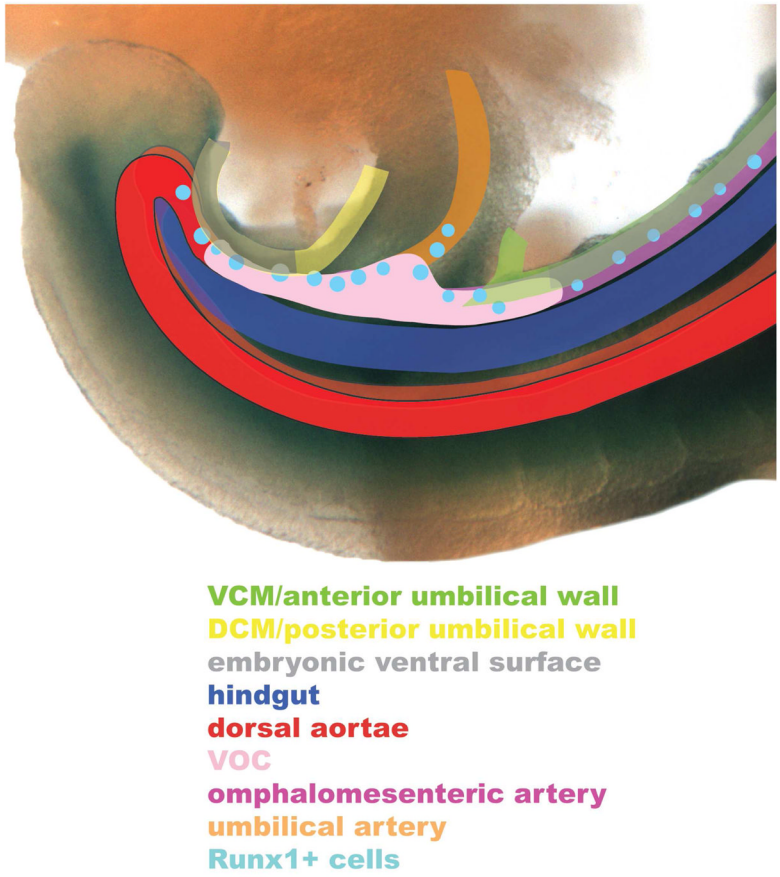

Fig. 12. Schematic diagram of the relationship between the umbilical and embryonic ventral surfaces, vessel of confluence, and posterior arterial system (~9.75 dpc, 23–27-s stage)

This schematic diagram, which was superimposed onto the posterior end of a Ptc-1-positive (blue color) embryo at ~9.75 dpc (~23–27-s), summarizes the ultimate relationship thus far identified between robust Ptc-1 sites described in this study. It excludes the venous system, and does not fully address the dorsal aortae, which have been dealt with in previous studies (Peeters et al., 2009; Yokomizo and Dzierzak, 2010). Note that the walls of the umbilical cord overlie the hemogenic vessel of confluence, from which the hemogenic umbilical and omphalomeseneteric arteries and dorsal aortae extend. See text for details. Abbreviations: al, allantois; cd, chorionic disk; s, somite; tb, tailbud. Ventral is up, dorsal is down.

TABLE 1

DESCRIPTION OF THE DEVELOPMENTAL EVENTS OBSERVED IN THIS STUDY

PHASE	MORPHOGENETIC EVENTS
Phase I (OB-HF, ~7.0–8.0 dpc)	• Emergence of allantoic bud; • Formation of proximal allantoic walls (VCM, DCM); • Onset of allantoic elongation and vasculogenesis; • Amnion, chorion and yolk sac blood islands in nascent states.
Phase II (1–9-s, ~8.0–8.75 dpc)	• Allantoic elongation and fusion with the chorion; • Patterning the nascent umbilical artery into a stem and branch structure; • Establishment of the VOC; • Amalgamation of the allantoic, yolk sac, and embryonic dorsal aortae at the VOC; • Hindgut invagination just anterior to VOC.
Phase III (10–27-s, ~8.75–9.75 dpc)	**Phase IIIa** (10–18-s; ~8.75–9.25 dpc): • Embryo turning; • Formation/extension of the hindgut tube and omphalomeseneteric artery (OA); • Appearance of the midline aorta; • Tailbud expansion; • VCM and DCM shift to occupy midline anterior (formerly VCM) and posterior (formerly VCM) ventral positions; • Formation of the umbilical ring. **Phase IIIb** (~23–27-s; ~9.75 dpc): • Expansion of the tailbud, hindgut tube and omphalomeseneteric artery; • Appearance of the midline aorta.

TABLE 2

COMPARISON OF X-GAL STAINING SOLUTIONS

	I $K_3Fe(CN)_6$	II $K_4Fe(CN)_6.3H_2O$	MgCl2	X-gal
Standard	5 mM	5 mM	2 mM	1 mg/ml
Iron Solution I	10 mM	0	2 mM	1 mg/ml
Iron Solution II*	0	10 mM	2 mM	1 mg/ml

*Iron solution II was found to be optimal for the detection of Ptc-1 in this study.

TABLE 3

FERTILITY AND GENOTYPE DISTRIBUTION FROM *Ptc1*^{tm1Mps}*/J* x WILDTYPE MATINGS

Genetic background	Percentage successful matings[1]	No. litters/breeding couple[2]	Average litter size ± SEM (average no. litters/pair)	No. Ptc1$^{+/+}$ offspring (%)	No. Ptch$^{+/-}$ offspring (%)	P-value[4]
Ptc1^{tm1Mps}*/J*	85.7	1.6	6.18 (2.11)	94 (65.2) [3]	50 (34.7) [3]	0.000246
Ptc1 (CBAC57Bl6)	75.0	3.9	7.91 (3.62)	197 (54.1)	167 (45.9)	0.116

[1] Successful mating was defined by the production of at least one litter over three months. 3 out of 21 Ptc1^{tm1Mps}/J couples never produced a litter, while 3 out of 12 outbred couples failed to breed.

[2] 21 breeding couples of *Ptc1*^{tm1Mps}*/J* background were maintained over an average of 171 days, producing 33 litters. The outbred *Ptc1* line of CBAC57Bl6 background consisted of 12 couples maintained over an average of 152 days, producing 47 litters.

[3] This number excludes four entire litters and at least 11 other pups that died prior to genotyping at 20 days. Autopsy of three dead *Ptc1*$^{+/-}$ male mice revealed respiratory problems (228 days old), a 0.5–1.5cm shoulder tumor (122 days old) and a hind leg tumor (403 days old). An intestinal tumor was also found in a pregnant 180-day-old *Ptc1*$^{+/-}$ female upon dissection of her litter. No abnormalities were detected in outbred *Ptc1*$^{+/-}$ heterozygous mice.

[4] Chi-squared test was used to analyze Mendelian inheritance.

TABLE 4

SEGREGATION RATIOS OF HETEROZYGOUS *Ptc1*$^{+/-}$ / TOTAL EMBRYOS FOR LOCALIZATION STUDIES AS DETERMINED BY X-GAL STAINING*

8.0 dpc	9.0 dpc	9.75 dpc
96/183 (20 litters) 52.5%	61/113 (14 litters) 54.0%	12/27 (3 litters) 44.4%

* Resorbed embryos, which did not exceed F2 background levels (data not shown), are not included in these numbers.